Chapter 12

Neuro-Fuzzy Data Normalization Applied for Impedance-based SHM to the Oil & Gas Industry

Chapter details

Chapter DOI:

https://doi.org/10.4322/978-65-86503-88-3.c12

Chapter suggested citation / reference style:

Freitas, Fernando A., et al. (2022). "Neuro-Fuzzy Data Normalization Applied for Impedance-based SHM to the Oil & Gas Industry". *In* Jorge, Ariosto B., et al. (Eds.) *Uncertainty Modeling: Fundamental Concepts and Models*, Vol. III, UnB, Brasilia, DF, Brazil, pp. 384–426. Book series in Discrete Models, Inverse Methods, & Uncertainty Modeling in Structural Integrity.

P.S.: DOI may be included at the end of citation, for completeness.

Book details

Book: Uncertainty Modeling: Fundamental Concepts and Models

Edited by: Jorge, Ariosto B., Anflor, Carla T. M., Gomes, Guilherme F., & Carneiro, Sergio H. S.

Volume III of Book Series in:

Discrete Models, Inverse Methods, & Uncertainty Modeling in Structural Integrity

Published by: UnB City: Brasilia, DF, Brazil Year: 2022

DOI: https://doi.org/10.4322/978-65-86503-88-3

Neuro-Fuzzy Data Normalization Applied for Impedance-based SHM to the Oil & Gas Industry

Fernando Augusto Freitas[1], Rosana Sueli da Motta Jafelice[2*], José Waldemar da Silva[2], Quintiliano S. S. Nomelini[2], Diogo de Souza Rabelo[3], José dos Reis V. Moura Jr[4], Roberto M. Finzi Neto[5], Carlos A. Gallo[5] and Julio E. Ramos[6]

[1]Math Graduate Program, Federal University of Uberlândia, Brazil. E-mail: fernandoaugusto.mat@gmail.com
[2]Faculty of Mathematics, Federal University of Uberlândia, Brazil. E-mail: rmotta@ufu.br; zewaldemar@ufu.br; quintiliano.nomelini@ufu.br
[3]Post-Graduate Program – Industrial Engineering, Fed. University of Goias, School of Sciences and Technology, Aparecida de Goiania, Brazil. e-mail: diogo.rabelo@ufg.br
[4]Post-Graduate Program – Modeling and Optimization, Fed. University of Catalao, Brazil. e-mail: zereis@ufcat.edu.br
[5]Post-Graduate Program – Mechanical Engineering, Federal University of Uberlandia, Brazil. e-mail: finzi@ufu.br; gallo@ufu.br
[6]Petrobras, Petroleo Brasileiro S.A., RD Center (CENPES), Brazil. e-mail: julio.ramos@petrobras.com.br

*Corresponding author

Abstract

The electromechanical impedance-based approach can perform Structural Health Monitoring (SHM). The impedance signature is used to map any structural change and for follow-up purposes. Two major challenges for SHM are normalizing the collected impedance data and determining strategies to assess the level of damage to engineering structures and equipment over time. The objectives of this chapter are to present a data normalization technique and to illustrate a case study by modeling the damage level of an aluminum beam using Fuzzy Rule-Based Systems (FRBSs) that are generated using the Adaptive Neuro-Fuzzy Inference System (ANFIS). The training is carried out for the first aim with the input variables temperature and frequency, and the output data are impedance baseline signatures. The temperature effect can generate changes in the impedance signature, leading to incorrect structural diagnoses. Because of that, it is necessary to compensate for the impact of this variable for later prediction of impedance signatures without damage at temperatures that were not necessarily observed in the data collection. Results were obtained in the validation, in which a part of the data was used for training the FRBSs, and another *part was intended for confirmation. Both of the baseline data indicate good accuracy of the predicted signatures since the highest Correlation Coefficient Deviation (CCD) damage index was* $0,003800021$. *To evaluate the damage level, FRBSs were constructed, with the input variables being two damage indices established by the electromechanical impedance signatures. The FRBSs average hit percentages are* 95%. *This result can indicate possible inputs for FBRSs to identify the damage levels when these FRBSs output values are unknown. Finally, the methodology proposed is used for the damage detection process in an experiment to detect corrosion-related damage in metallic structures. .*

Keywords: Electromechanical impedance-based SHM; Fuzzy sets; ANFIS; Data normalization; Damage detection

1 Introduction

The Electromechanical Impedance-based Structural Health Monitoring technique (EMI-SHM) allows detecting structural changes using PZT (Lead Zirconate Titanium) ceramic transducers, bonded or embedded in the evaluated host structure. This technique reduces direct and indirect maintenance costs through an online and near real-time monitoring approach. It is also possible to improve by detecting design mistakes in their developing stage. This is possible by allowing a change of potential changes through a shift in excitation that can be changed. These changes are changed to qualitative parameters and can be tested through pattern models, which are either tested pure or untested curvature indices or tested as basal curvature with a verified curvature in the current state [Rabelo et al., 2017] EMI-SHM can be applied to complex structures, such as [Maruo et al., 2015] aircraft panels, steel fiber reinforced concrete structures [Silva et al., 2020] and other types of applications.

This technique has several advantages that make it promising, such as it can be applied to complex structures; transducers can be installed in hard-to-reach places; it has a high sensitivity to incipient failures; measurement data is easy to interpret; it can be implemented online; and is adapted for continuous monitoring, which can reduce the number of maintenance stops [Park et al., 1999].

However, an important limitation of this technique is the choice of the ideal frequency band used for the monitoring process. This parameter is usually determined experimentally in the signature range with high peak density, indicating good electromechanical coupling. It is worth noting that the width of the frequency band can influence the ability to detect structural faults, so a very narrow band can limit the variety of detectable damage types. On the other hand, an extensive frequency range may contain regions of low electromechanical coupling, and small changes may not be found in a specific part of the frequency range, due to a low local electromechanical coupling [Rabelo et al., 2017]. Therefore, it is necessary to use several frequency points and assume that, at least in some of them, the impedance will be modified in the presence of damage. Alternatively, the frequency range can also be determined using artificial intelligence techniques [Moura and Steffen, 2004].

Thus, EMI-SHM allows the early detection of structural failures, which can increase work environment safety and reduce maintenance costs. The presence or absence of structural modifications, in general, is verified from damage indices or metrics computed from the comparison between reference signatures, known as baseline, and investigated signatures.

Among the various existing damage indices or metrics, RMSD1 (root mean square deviation), CCD (correlation coefficient deviation), and ASD (mean square difference) [Palomino, 2008] can be mentioned. The RMSD1 index can be calculated through the equation (1), the ASD through the equation (2), while the CCD is computed by (3), which also involves the difference between one and the correlation coefficient (CC), given by the equation (4), as follows:

$$RMSD1 = \sqrt{\sum_{j=1}^{n} \frac{(Z_{B,j} - Z_{I,j})^2}{Z_{I,j}^2}}, \tag{1}$$

$$ASD = \sum_{j=1}^{n} [(Z_{B,j} - Z_{I,j}) - (\bar{Z}_B - \bar{Z}_I)]^2, \tag{2}$$

$$CCD = 1 - CC, \tag{3}$$

$$CC = \frac{1}{n} \sum_{j=1}^{n} \left\{ \frac{\left[Z_{B,j} - \bar{Z}_B\right]\left[Z_{I,j} - \bar{Z}_I\right]}{S_{Z_B} S_{Z_I}} \right\}, \tag{4}$$

where $Z_{B,j}$ is the real part of the baseline signature at frequency j and $Z_{I,j}$ is the real part of the investigated signature at frequency j, both considering n frequency points, $\bar{Z}_B$ and $\bar{Z}_I$ are the averages of the baseline and investigated signatures, respectively, in the selected frequency range, S_{Z_B} is the standard deviation of the baseline signature and S_{Z_I} is the standard deviation of the investigated signature, considering all frequency points of each one.

Suppose the structure does not show significant changes at the time of investigation regarding the state of the baseline signature. In that case, it is expected that the damage index determined from the two signatures will be relatively small.

Fluctuations or changes in the impedance signature due to factors other than the damage itself can inflate the damage index, leading to a false diagnosis. This is especially true if temperature changes are not adequately compensated for, which can lead to false positives as to the presence of damage. Therefore, it is necessary to use methodologies that compensate for temperature effects so that the impedance changes detected in the analysis are mainly due to structural changes and not environmental impacts.

The term data normalization in SHM systems refers to a data processing procedure, which may include variations caused in the impedance signatures due to environmental and operational effects. There are many studies on the normalization of electromechanical impedance signatures, such as Krishnamurthy et al. [1996]; Bhalla et al. [2003]; Zhou et al. [2009]; Sepehry et al. [2011] and Bastani et al. [2012], whose results can be applied under specific conditions. There are also other studies such as Sun et al. [1995], Park et al. [1999] and Koo et al. [2009] on the correction of the variation of the impedance signature caused by the temperature effect, maximizing the correlation between the baseline signature and the signature measured for investigation of the structure. In these approaches, a necessary condition for model validation is that a baseline signature at a specific temperature level must be stored to be used for compensation purposes. Due to weather or climate constraints, this can be an important limitation if impedance signature(s) were not stored at a given temperature during the baseline acquisition procedure.

A technique to remove the temperature effect, based on the fit of regression polynomials, is proposed in Gianesini et al. [2021]. However, applying this technique is conducted in two steps: the first to adjust the horizontal displacement of the signature and the second to adjust the vertical.

However, these techniques have limitations, such as the size of the frequency band and, in the case of adjustment via regression analysis, there are assumptions to be taken into account, such as homogeneity, normality, and independence on the model residuals, which is not always possible to guarantee, and therefore the normalization of the data would be compromised.

Another critical difficulty encountered in traditional SHM methodologies is quantifying damage from these metrics obtained at their respective temperatures since there is no information on whether the behavior of the damage increment and metric values are or are not directly linked.

Thus, the main objective of this chapter is to present an alternative for the normalization of electromechanical impedance data and a way to quantify the possible structural changes. To this end, we propose using Fuzzy Rule-Based Systems (FRBSs), a methodology that enables the manipulation of uncertain information or the mathematical representation of imprecision. This chapter is based on Freitas [2021].

The mathematical tool used in modeling the problems under study is the theory of Fuzzy Sets, which was proposed by Zadeh [1965]. This theory has proved to be an efficient mathematical tool for quantifying and characterizing uncertainties in various contexts. To exemplify, in the work of Ferreira [2011], the mathematical modeling of luminescence is carried out from experiments with a beam of light focused on a point on the surface of a glassy sample; in Nardez [2015], it is required the determination and positioning of points with high accuracy, using the Global Navigation Satellite System (GNSS), in which it is necessary to know the phase center displacements of the antennas GNSS; in the work of Alfaro [2019], the dynamics of delayed Human Immunodeficiency Virus (HIV) under antiretroviral treatment in seropositive individuals with two fuzzy parameters is simulated. In the first two works, ANFIS was used to determine SBRFs applied in modeling these phenomena.

In the building and elaboration of FRBSs, there is a need for the help of a specialist in the area to find its best configuration and development of its rules. Thus, ANFIS [Fresno et al., 2015] has proved to be an exciting tool as an aid for this FRBS configuration step when the data of the input and output variables are known.

Thus, this chapter aims to determine the FRBSs through ANFIS that make possible the normalization of electromechanical impedance data (Part I) and damage identification (Part II).

- Part I, which deals with normalization, took place in two steps, given by:

Step 1: (**Validation of FRBSs**) In this phase, the baseline impedance signatures are divided into two distinct groups. One group is used for training the model and the other for validation. The validation of the FRBS is performed through some damage metric; the CCD, for example, is calculated from a signature that was left out of training and the corresponding baseline signature built from the FRBSs and, therefore, both at the same temperature. It is noteworthy that the objective is to create baseline signatures and, therefore, it is expected that the damage metrics, under the hypothesis of model validity, will be low because they are comparisons between signatures that represent the structure in the same state, that is, baseline status;

Step 2: (**Building baseline signatures**) The second step consists of determining new FRBSs, taking into account all signatures collected in the baseline stage. These FRBSs build baseline signatures at any temperature, even if not measured but within the collection range. Thus, the problem of the lack of equivalence of the temperature effect between the baseline signatures and the signatures in the investigation step is solved through the FRBSs obtained by ANFIS.

- Part II deals with the identification of the damage level and consists of initially computing the values of the metrics RMSD1 (equation (1)) and CCD (equation (3)) and, from that, using these metrics as FRBS inputs, perform training through ANFIS to generate the FRBS that can identify the level of damage in the structure.

To meet the objectives proposed above, section 2 presents the main concepts of fuzzy set theory, which underlie the uncertainty found in FRBSs, and an example that illustrates this methodology, used in the context of electromechanical impedance at detecting levels of damage. Section

3 presents the primary tool for obtaining the FRBSs built in this work, ANFIS. Section 4 offers a proposal, in the form of an application, for data normalization. In section 5, another application is presented to investigate the structure's level of damage. Finally, in section 6, the conclusions of the chapter are presented.

2 Fuzzy Sets Theory

The fuzzy sets theory was initially proposed by Zadeh [1965], aimed at modeling uncertain situations. Thus, unlike classical set theory, which determines in a very well-defined way the insertion of an element in the set or not, in fuzzy logic, the elements are inserted in the groups with their respective degrees of membership, according to Pourjavad and Shahin [2018]. Thus, a fuzzy set is used to present vague concepts in the characterization of models mathematically.

The following section provides a formal definition of this concept and some examples, according to Jafelice et al. [2012], Barros and Bassanezi [2015].

2.1 Fuzzy Sets

Definition 2.1 *A set fuzzy A of the universe U is characterized by a membership function: $\mu_A : U \to [0,1]$. This is called the membership function of the set fuzzy A. The value $\mu_A(x)$ of the function is interpreted as the degree to which the element x belongs to the set fuzzy A, that is, $\mu_A(x) = 0$ indicates a no membership of x to A, and $\mu_A(x) = 1$ indicates total membership of the set [Zadeh, 1965]. A classical set of ordered pairs can also represent a set fuzzy: $A = \{(x, \mu_A(x))|x \in U\}$.*

In this context, the intention is to establish, for each element of a set, a value between 0 and 1, which is considered the membership degree and serves to express how much the element belongs or not to a subset of this set. The membership function can be triangular, trapezoidal, Gaussian, or even have other geometric shapes [Barros and Bassanezi, 2015].

Definition 2.2 *A singleton set is a fuzzy set with a membership function that is unity at a single point in the considered universe and zero elsewhere.*

When it comes to fuzzy sets, it is possible to think about operations that can be performed in this context. Thus, the union, intersection, and complement operations of classical sets can be applied to fuzzy sets and will be covered in the following subsection.

2.2 Operations with Fuzzy Sets

Definition 2.3 *Given A and B two fuzzy sets with μ_A and μ_B their respective membership functions, one can define the union operations (5) (Figure 1b), intersection (6)(Figure 1c) and complementary (7)(Figure 1d) of the sets fuzzy A and B, for all $x \in U$, given by:*

$$\mu_{(A\cup B)}(x) = \max\{\mu_A(x), \mu_B(x)\}, \tag{5}$$

$$\mu_{(A\cap B)}(x) = \min\{\mu_A(x), \mu_B(x)\}, \tag{6}$$

$$\mu_{A'}(x) = 1 - \mu_A(x), \tag{7}$$

where 1 represents the constant function.

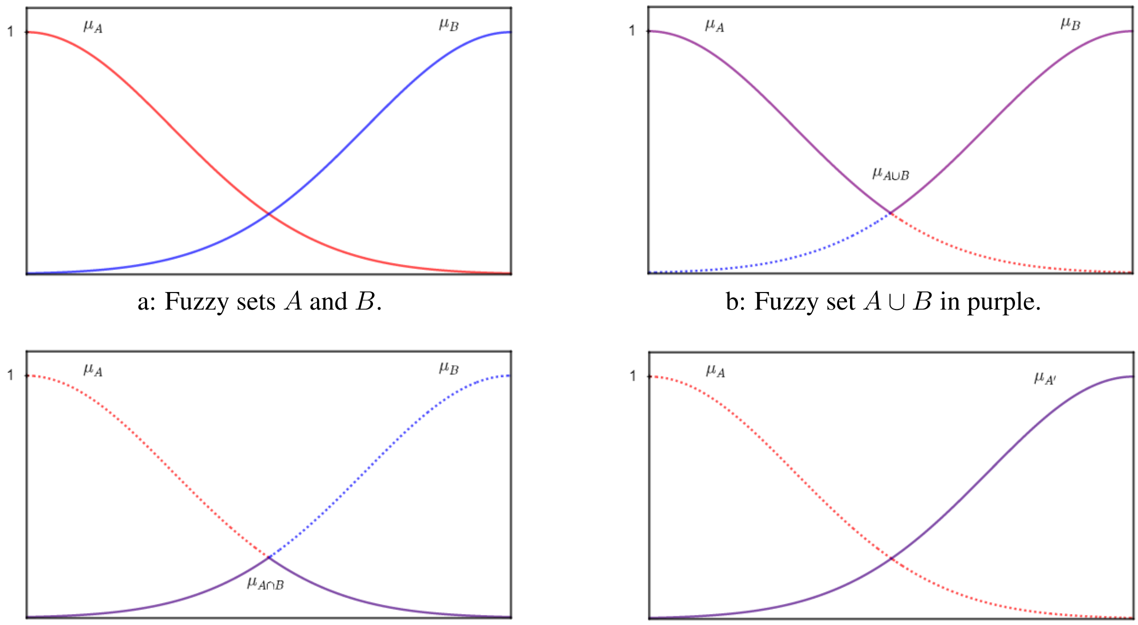

a: Fuzzy sets A and B.

b: Fuzzy set $A \cup B$ in purple.

c: Fuzzy set $A \cap B$ in purple.

d: Complementary fuzzy set A' in purple.

Figure 1: Representation of operations on fuzzy sets through membership functions. Source: Freitas et al. [2021c].

In the next subsection, the triangular norms are defined.

2.3 Triangular Norms

Definition 2.4 *A triangular conorm (s-norm) is a binary operation* $s : [0, 1] \times [0, 1] \to [0, 1]$*, denoted by* $s(x, y) = xsy$ *, satisfying the following conditions:*

- *Commutativity:* $xsy = ysx$*;*
- *Associativity:* $xs(ysz) = (xsy)sz$*;*
- *Monotonicity: If* $x \leqslant y$ *and* $w \leqslant z$ *then* $xsw \leqslant ysz$*;*
- *Boundary conditions:* $xs0 = x$ *and* $xs1 = 1$.

Example 2.1

a) Standard Union: $s : [0, 1] \times [0, 1] \to [0, 1]$ *with* $xsy = \max(x, y)$*, (Figure 2a);*

b) Algebraic Sum: $s : [0, 1] \times [0, 1] \to [0, 1]$ *with* $xsy = x + y - xy$*, (Figure 2b);*

c) Limited Sum: $s : [0.1] \times [0.1] \to [0.1]$ *with* $xsy = \min(1, x + y)$*, (Figure 2c);*

d) Drastic Union: $s : [0, 1] \times [0, 1] \to [0, 1]$ *com*

$$xsy = \begin{cases} x & \textit{if } y = 0; \\ y & \textit{if } x = 0; \\ 1 & \textit{otherwise;} \end{cases} \quad \textit{(Figure 2d).}$$

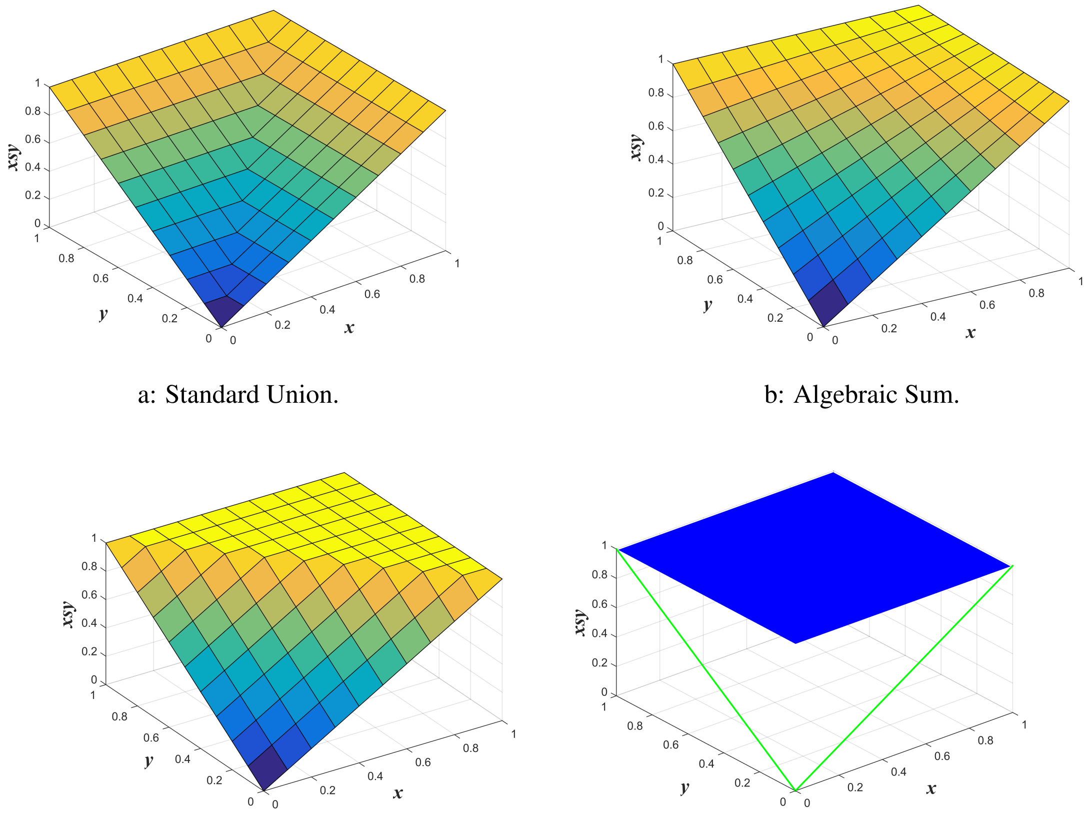

a: Standard Union.

b: Algebraic Sum.

c: Limited Sum.

d: Drastic Union.

Figure 2: Representation of the surfaces generated by the examples of s-norms. Source: Freitas et al. [2021c].

Definition 2.5 *A triangular norm (t-norm) is a binary operation* $t : [0,1]\times[0,1] \to [0,1]$*, denoted by* $t(x,y) = xty$*, satisfying the following conditions:*

- *Commutativity:* $xty = ytx$*;*
- *Associativity:* $xt(ytz) = (xty)tz$*;*
- *Monotonicity: If* $x \leqslant y$ *and* $w \leqslant z$ *then* $xtw \leqslant ytz$*;*
- *Boundary conditions:* $0tx = 0$ *and* $1tx = x$*.*

Example 2.2

a) Standard Intersection: $t : [0,1] \times [0,1] \to [0,1]$ *with* $xty = \min(x,y)$*, (Figure* **??***);*

b) Algebraic Product: $t : [0,1] \times [0,1] \to [0,1]$ *with* $xty = xy$*, (Figure 3b);*

c) Limited Difference: $t : [0,1] \times [0,1] \to [0,1]$ *with* $xty = \max(0, x+y-1)$*, (Figure 3c);*

d) Drastic Intersection: $t : [0,1] \times [0,1] \to [0,1]$ *with*

$$xty = \begin{cases} x & \text{if } y = 1; \\ y & \text{if } x = 1; \\ 0 & \text{otherwise;} \end{cases} \quad \text{(Figure 3d).}$$

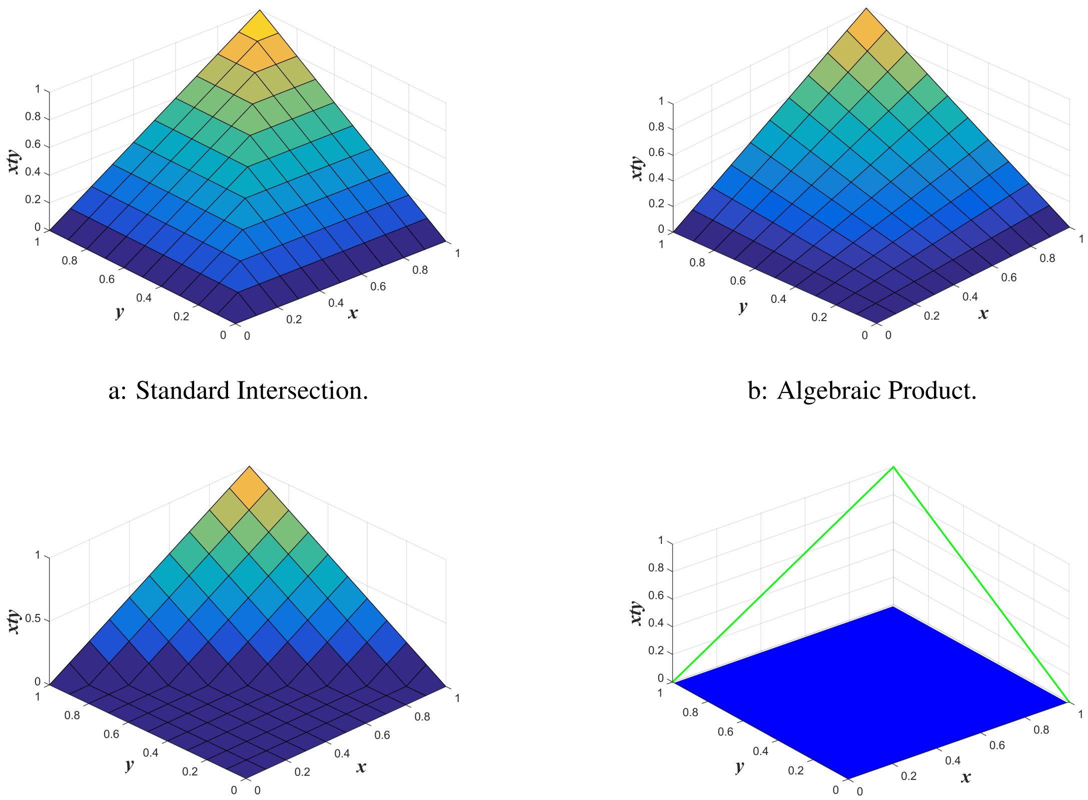

a: Standard Intersection.

b: Algebraic Product.

c: Limited Difference.

d: Drastic Intersection.

Figure 3: Representation of the surfaces generated by the examples of t-norms. Source: Freitas et al. [2021c].

Next, an essential technique of fuzzy set theory for this work, the fuzzy rule-based systems, is discussed.

2.4 Fuzzy Rule-Based System

The Fuzzy Rule-Based System (FRBS) is a process of mapping an input set to an output set. To introduce an FRBS, it is necessary to define linguistic variables.

2.4.1 Linguistic Variables

According to Jafelice et al. [2012], linguistic variables are used to quantify data or information using expressions of human communication.

Definition 2.6 *A linguistic variable is a variable whose value is expressed qualitatively by a linguistic term, providing a concept to the variable and quantitatively through the membership function. Thus, the linguistic variable is composed of a symbolic variable and a numerical value.*

Example 2.3 *Considering the linguistic variable structural change in aluminum plate, ranging from* 0 *to* 1*, its linguistic terms are assumed as small, medium, and large. These values are represented by fuzzy sets as shown in Figure 4.*

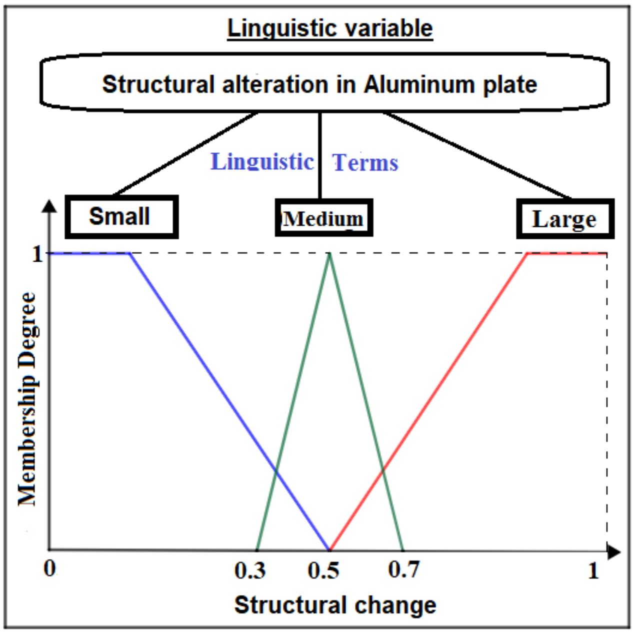

Figure 4: Linguistic variable structural change in an aluminum plate. Source: Adapted from Freitas et al. [2021c].

With the definition of linguistic variables, one can go further to the concept and structuring of FRBS, which will be done in the following subsection.

2.4.2 FRBS

An FRBS is composed of four components: the input processor (fuzzification process), a rule base, a fuzzy inference method, and an output processor (defuzzification process), which are connected as shown in Figure 5.

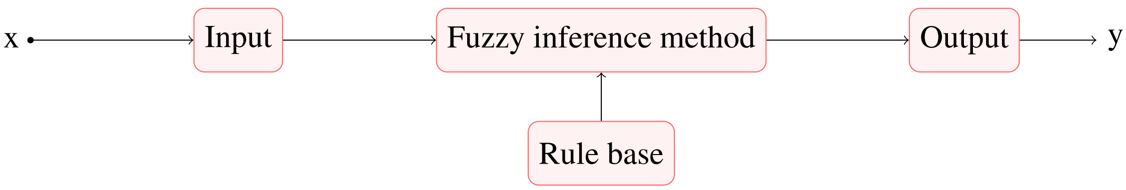

Figure 5: FRBS architecture.

Each component is defined as:

- Input Processor (Fuzzification) The system inputs are translated into fuzzy sets in their respective domains in this component.
- Rule Base This component, together with the inference method, can be considered the core of fuzzy rule-based systems. This is composed of a collection of fuzzy propositions described in the linguistic form:

$$\text{If } x_1 \text{ is } A_1 \text{ and } x_2 \text{ is } A_2 \text{ and } \ldots \text{ and } x_n \text{ is } A_n$$
$$\text{then } y_1 \text{ is } B_1 \text{ and } y_2 \text{ is } B_2 \text{ and } \ldots \text{ and } y_m \text{ is } B_m,$$

where $A_1, \ldots, A_n$ are the fuzzy input sets and $B_1, \ldots, B_n$ are the fuzzy output sets.

- Fuzzy Inference Method
  It is in this component that each fuzzy proposition is mathematically translated using approximate reasoning techniques. Mathematical operators will be selected to define the rule base's fuzzy relationship. In this way, the fuzzy inference machine is of fundamental importance for the success of the fuzzy system, as it provides the output from each input fuzzy and the relationship defined by the rule base.

  – Mamdani Method
    A rule is characterized by If (antecedent) then (consequent), provided by the Cartesian product fuzzy of the fuzzy sets that compose its antecedent and consequent. Mamdani's method groups the logical OR operator, arranged by the maximum operation in the s-norm, and the AND operator, configured by the minimum operation in the t-norm, in each rule, as shown in Figure 6. Given the following rules:

Rule 1: If (x_1 is A_1 and x_2 is B_1) then (y is C_1);
Rule 2: If (x_1 is A_2 and x_2 is B_2) then (y is C_2).

In Figure 6 the output y is represented through the Mamdani inference method for the inputs x_1 and x_2, using the max-min composition.

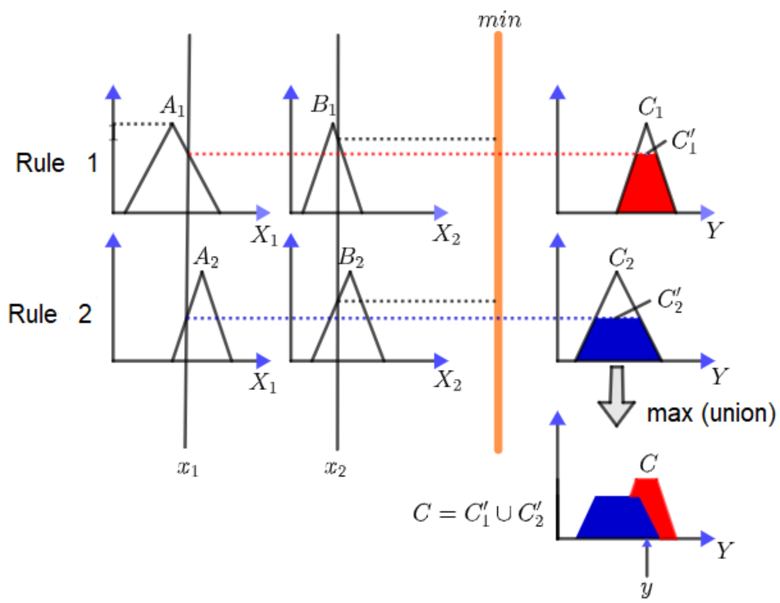

Figure 6: Mamdani inference method with max-min composition. Source: Adapted from Freitas et al. [2021c].

  – Takagi-Sugeno method
    The consequence characterizes this method in that each rule is a function depending on the input variables. Therefore, given the inputs, x_1 and x_2, the output for each rule is given as a linear combination of these inputs. Thus, given the following rules:

Rule 1: If (x_1 is A_1 and x_2 is B_1) then ($y = f_1(x_1, x_2)$);
Rule 2: If (x_1 is A_2 and x_2 is B_2) then ($y = f_2(x_1, x_2)$).

A representation of the output y, obtained from this inference method (Takagi-Sugeno), for the inputs x_1 and x_2, with $k_{ij} \in \mathbb{R}$, $i = 1, 2$ and $j = 0, 1, 2$, is shown in Figure 7

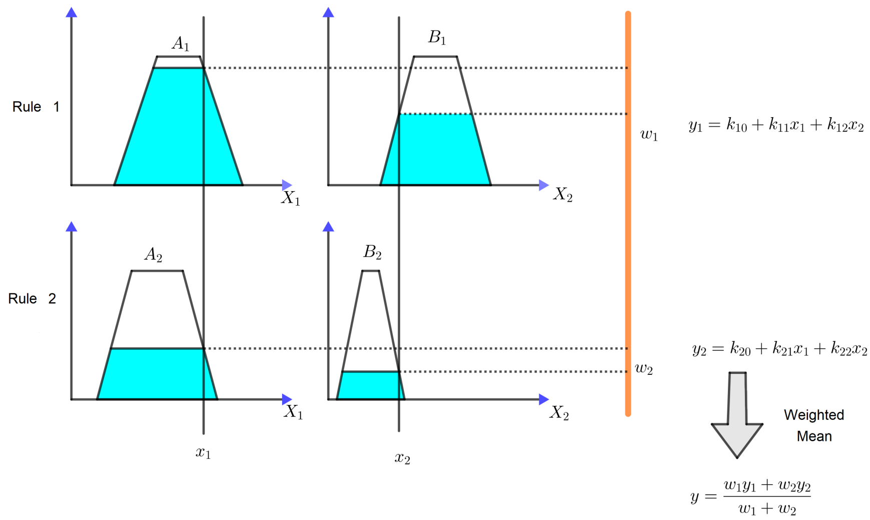

Figure 7: Takagi-Sugeno inference method. Source: Adapted from Freitas et al. [2021c].

The generalization of these inference methods can be found in Barros and Bassanezi [2015].

- Output Processor (Defuzzification)
  defuzzification is a process that allows representing a set fuzzy by a crisp number. In fuzzy systems, in general, the output is a fuzzy set. Thus, we must choose a method to defuzzify the output and obtain a real number representing it. The most common method of defuzzification is as follows:

  – Center of gravity
    This defuzzification method is similar to the weighted average for data distribution, with the difference that the weights are the values $\mu_C(y_i)$ that indicate the degree of compatibility of the value y_i with the concept modeled by the fuzzy C set.
    For a discrete domain, we have:

$$G(C) = \frac{\sum_{i=0}^{n} y_i \mu_C(y_i)}{\sum_{i=0}^{n} \mu_C(y_i)}, \tag{8}$$

    where y_i belongs to the domain of C.

The following section will present an example of a system based on fuzzy rules using Mamdani's inference method.

2.5 FRBS Example: Grinding of Aluminum Beams

The experiment used to obtain the sampled data was carried out on aluminum beams. The structural modification was caused by the grinding process, which is the mechanical wear of the structure. The data set were obtained using the electromechanical impedance-based SHM technique, so that the experiment was carried out in a climatic chamber, as shown in Figure 8, with temperature and humidity control, at the Structural Mechanics Laboratory (LMEst) of Faculty of Mechanical Engineering of the Federal University of Uberlandia. This experiment was chosen due to the increasing behavior, from the third cycle, of the metrics referring to the electromechanical impedance data set obtained, a condition that occurs, in general, in the actual SHM.

Figure 8: Climatic chamber used in the experiment. Source: Freitas et al. [2021c].

2.5.1 The Experimental Setup

In this experiment, four aluminum beam structures were used. The aluminum beams are 500mm long, 38mm wide, and 3.2mm thick. In each of them, a 1 mm thick and 20 mm diameter PZT patch was bonded 100 mm from the edge of the structure.

The failure mechanisms, or simulated damage, used in the experiment were surface grinding on one of the faces of the 30mm wide beams at 70mm from the opposite end and the same face on which the PZT patch was bonded. Nine levels of damage were considered in total, two baseline and seven levels of thickness removal by machining. Specimen 4 was used as a control mechanism, being removed from the chamber along with the others, but no failure mechanism was introduced in it. The difference between the mass values for specimen 4 (Table 1) comes from a failure in the measurement mechanism since the integrity of the beam was not altered in this case.

Figure 9 shows the four specimens tested in the bi-supported boundary condition. The beams were supported under the thickness, not over the width.

Figure 9: Specimens used in the test. Source: Freitas et al. [2021c].

It is important to emphasize that the stands for positioning the structures inside the chamber were printed in ABS plastic, with rounded feet, to reduce the interference of the chamber floor in the structures and make it possible to embed connectors in the specimens themselves. The structures were removed from inside the chamber for machining and returned to the chamber for continuity of measurements with the least possible interference from the cables since they were placed in the same position inside the chamber, as shown in Figure 10.

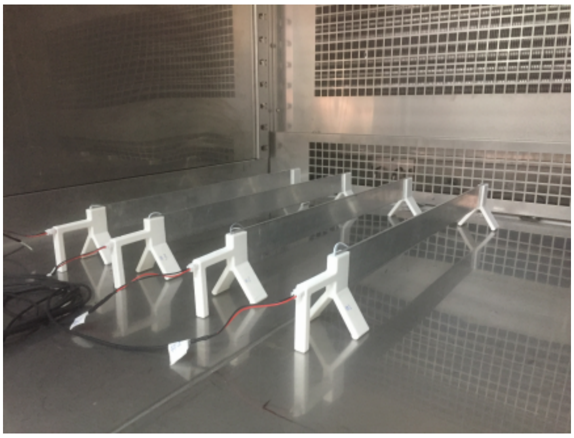

Figure 10: Positioning the specimens inside the chamber. Source: Freitas et al. [2021c].

The temperature range increased with an increment of $3\,°C$, in the range of 13 to $40\,°C$; therefore, the measurements were obtained at ten different temperatures or in ten cycles.

For each configuration: specimen, temperature, and damage condition, samples of size 30 were obtained. Thus, in a total of 10 temperature cycles, nine damage levels, four specimens, and 30 repetitions, 10800 impedance signatures were gathered.

Since inserting damage was performed manually from a grinder, it was decided to adopt two variables as the response of each specimen after inserting the damage. The first answer is the mass, considering the mass loss from the previous state. For this answer, a precision balance of two decimal places of the gram was used, and eight measurements were taken to obtain the average. The second answer is the thickness in the region delimited for machining, considering the loss of thickness in the previous state. A gauge with a resolution of 0.01mm was used for the second answer. The average of 10 random measurements of the thickness of the area delimited by the machining was recorded. An image of one of the experimental conditions or machining levels is shown in Figure 11, which shows the distance between the edge point and the machined region.

The results of the mass measurements for each specimen are presented in Table 1 and for the thicknesses in each specimen in Table 2, which consist of eight conditions since the baseline con-

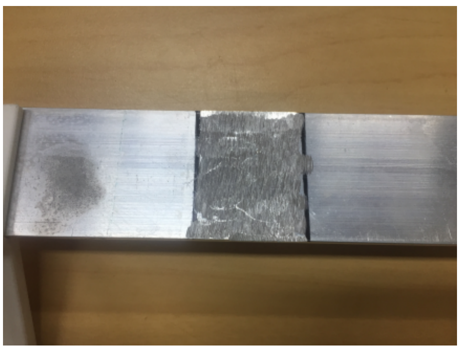

Figure 11: Damage 2 on specimen 1. Source: Freitas et al. [2021c].

dition was placed in the same parameter because they have the same data. In this experiment, we have the data of each damage attributed to the structure through the measurements of mass and thickness; however, the SHM technique is used to verify the structural change from the electromechanical impedance data set without worrying about the values presented in the tables. Thus, these values show that this experiment's loss of mass and thickness was slight.

Table 1: Mass, in grams, of specimens at each damage level.

Damage	Specimen			
	1	2	3	4
No damage [a]	191 .36	192 .42	192 .86	195 .89
1	191 .20	192 .27	192 .69	-
2	191 .16	192 .02	192 .58	-
3	190 .95	191 .82	192 .39	-
4	190 .41	191 .48	192 .02	-
5	189 .96	190 .54	191 .33	-
6	189 .16	189 .42	189 .78	-
7	187 .44	188 .57	188 .37	195 .83

[a] Baseline condition

Source: Adapted from Freitas et al. [2021c].

Table 2: Thickness, in millimeters, of the specimens at each damage level.

Damage	Specimen			
	1	2	3	4
No damage [a]	3.17	3.17	3.19	3.18
1	3.09	3.11	3.09	-
2	3.01	2.96	2.99	-
3	2.97	2.93	2.95	-
4	2.85	2.85	2.89	-
5	2.72	2.49	2.63	-
6	2.44	2.23	2.09	-
7	1.93	1.92	1.83	3.18

[a] Baseline condition

Source: Adapted from Freitas et al. [2021c].

As can be seen in all structures, by Table 2, the damages inserted in the three specimens never exceeded 50% of the thickness, and the last two machining levels applied were more severe to observe this more remarkable growth (more minor and greater progressions) in thickness loss. The electromechanical impedance technique seeks to analyze structural change; however, when the change is minimal, as found for the initial damages of the experiment, the methodology through the metrics may not show such a structural change. When this change was not included, the structural modification was considered irrelevant. The metric had a value very close to the structure metrics, comparing signatures in the baseline state.

Data from PZT1 patch were not used in the analysis due to problems in acquiring signatures.

2.5.2 Criteria for evaluation and design of FRBSs

A significant difficulty in obtaining FRBSs for damage classification is the enormous variability of signatures according to the material used and experiment settings. An experiment set up in close conditions can vary greatly in its signatures. This interference is smaller in metrics determined from these signatures, which justifies the use of CCD and ASD (Figure 12).

Then, the FRBS was built considering CCD and ASD metrics as input variables.

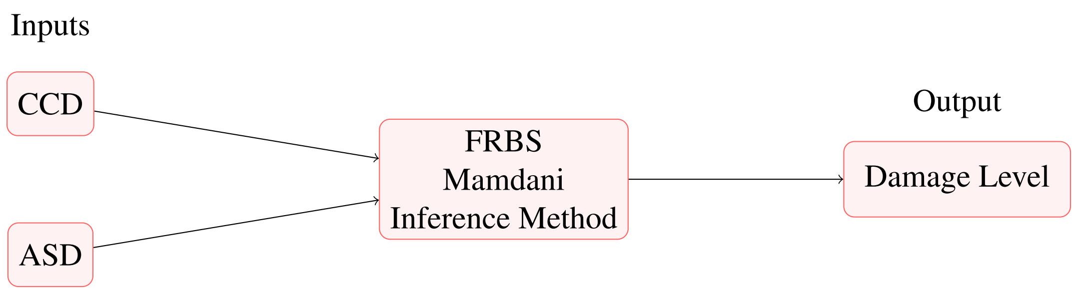

Figure 12: FRBS architecture.

To assess the quality of the FRBS, the combination of CCD and ASD metrics was used to determine the damage that each combination assumes. Three linguistic terms were designed for the damage level output variable: irrelevant, low, and medium. There was no characterization of high damage because the damage to the structure did not exceed 50% change from the original state when looking at the Table 2 of the thickness of the specimens.

2.5.3 Results of the Model Evaluation Step

Considering the experiment data for PZT2 and PZT3 patches, the CCD and ASD metrics were calculated from the baseline signatures and those investigated. For the output variable, damage level, the irrelevant linguistic term corresponds to the signature baseline and damages 1, 2, and 3; the small to damage 4 and 5; and the medium to 6 and 7, where the damages from 1 to 7 are those in Table 1.

In Figure 13, the numbers 1 and 2 on the abscissa axis represent baseline experimental condition measurements, and the numbers 3 to 9 are the actual damage, listed in this text, from 1 to 7.

For the construction of the FRBS, CCD and ASD metrics were considered for the inputs, as mentioned, due to the similar behavior of these two metrics, along with the damage, as shown in Figure 13.

From the analysis of the behavior of the CCD and ASD metrics, for PZT2 patch, trapezoidal membership functions were established for each input and output, which are given by:

- Inputs, as shown in Figure 14:
  - CCD values: the domain $[0, 0.1]$, representing the ranges $[0.0.025]$, $[0.02, 0.045]$ and $[0.04, 0.1]$, with the linguistic terms: Low, Medium and High, respectively.

  - ASD values: the domain $[1.2 \times 10^6, 3.5 \times 10^7]$, representing the ranges $[1.2 \times 10^6, 7,089 \times 10^6]$, $[6.09 \times 10^6, 1.2 \times 10^7]$ and $[1.1 \times 10^7, 3.5 \times 10^7]$, with the linguistic terms: Low, Medium and High, respectively.

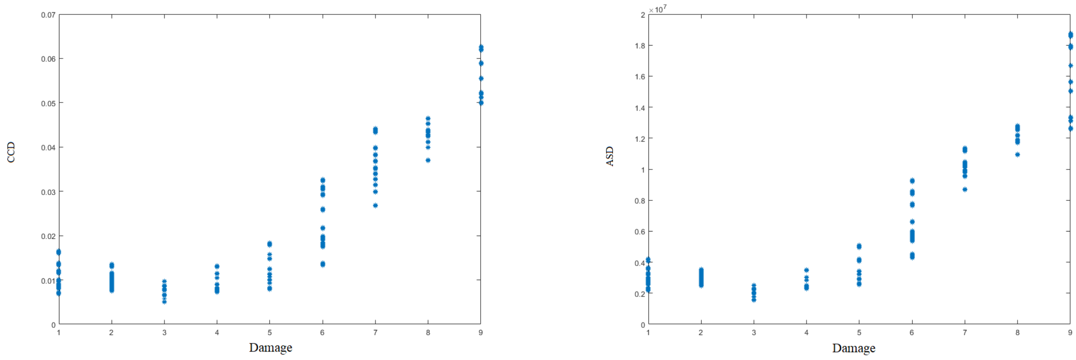

a: CCD metric behavior according to damage. b: ASD metric behavior according to damage.

Figure 13: Behavior of CCD and ASD metrics with respect to damage. Source: Adapted from Freitas et al. [2021c].

- Output Values: the domain $[0, 2]$, represented by functions singleton in 0, 1 and 2, with the linguistic terms: Irrelevant, Small and Medium, respectively, as shown in Figure 15.

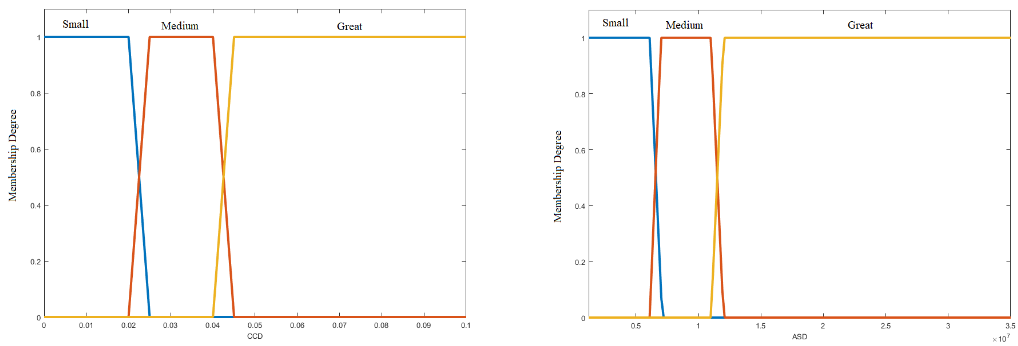

a: Membership function for the CCD variable. b: Membership function for the ASD variable.

Figure 14: Membership functions for the FRBS inputs. Source: Adapted from Freitas et al. [2021c].

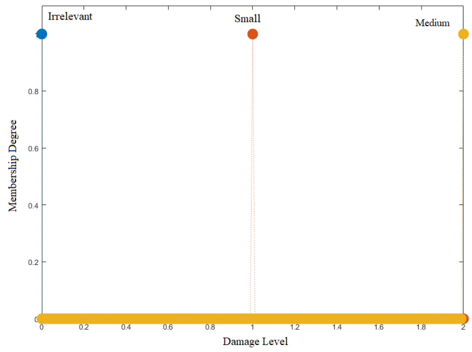

Figure 15: Membership functions for the FRBS output. Source: Adapted from Freitas et al. [2021c].

The following fuzzy rules were established:

Rule 1 :	If (CCD is **Low**) and (ASD is **Low**)	then the Damage Level is **Irrelevant**;
Rule 2 :	If (CCD is **Low**) and (ASD is **Medium**)	then Damage Level is **Irrelevant**;
Rule 3 :	If (CCD is **Low**) and (ASD is **High**)	then Damage Level is **Small**;
Rule 4 :	If (CCD is **Medium**) and (ASD is **Low**)	then Damage Level is **Irrelevant**;
Rule 5 :	If (CCD is **Medium**) and (ASD is **Medium**)	then Damage Level is **Small**;
Rule 6 :	If (CCD is **Medium**) and (ASD is **High**)	then Damage Level is **Medium**;
Rule 7 :	If (CCD is **High**) and (ASD is **Low**)	then Damage Level is **Small**;
Rule 8 :	If (CCD is **High**) and (ASD is **Medium**)	then Damage Level is **Small**;
Rule 9 :	If (CCD is **High**) and (ASD is **High**)	then Damage Level is **Medium**.

Data validation was performed by comparing the level of damage generated by the FRBS and that expected through the experiment by the absolute value of the difference between the level of damage obtained by the FRBS with that of the investigation. If this value is less than 0.5, it is compatible with the expected linguistic term. Otherwise, it is considered incompatible.

For the PZT2 patch data, the accuracy of 92.21% was found, showing that the methodology could identify the level of damage for a complex problem in most of the data. This same SBRF was used to verify the damage level for the PZT3 patch, and it was found that this sensor had a hitting percentage of 81.93%. Thus, the global hit level, regardless of the two PZT patches, was 87.03%, which is satisfactory, given the difficulty in performing such an analysis.

In the section 3, presented below, the theoretical foundation of ANFIS and relevant examples of numerical methods used for its computational implementation are discussed.

3 Fuzzy Rule-Based System on Adaptive Network

According to Fonseca [2012], the Adaptive Neuro-Fuzzy Inference System (ANFIS) is a hybrid technique of artificial intelligence that infers knowledge using fuzzy set theory principles and adds to this structure the possibility of learning inherent to artificial neural networks. Thus, this hybrid system solves one of the biggest problems of using fuzzy set theory: tuning the input and output functions of an FRBS. This section presents an explanation of artificial neural networks and ANFIS.

3.1 Artificial neural networks

Artificial Neural Networks (ANNs) can be seen as a computational method that, through experience, acquires knowledge based on the structure of biological neurons in the human brain, as shown in Figure 16.

The human brain is a parallel processing system that, even if the processing of an individual neuron is slow, is capable of processing trillions of operations simultaneously [Bezerra, 2016].

According to Valenca [2008], the biological neuron (Figure 16) is composed of a cell body, from which branches, known as dendrites, come out. The cell body and the telodendron, known as the terminal, are connected by the axon. The nerve impulse transmission between two neurons occurs from the axon of one neuron to the dendrite of the next, always in that order. The region where impulse transmission occurs is known as a synapse.

An important concept to understand the functioning of the biological neuron is the intensity of the stimulus, called the excitatory threshold, from which the neuron fires, or not, the nerve impulse. Therefore, if the stimulus is too small, its intensity will be below the excitatory threshold, and no nerve impulse will occur. On the other hand, after this threshold, the neuron's action potential will always be the same, whatever the intensity of the stimulus.

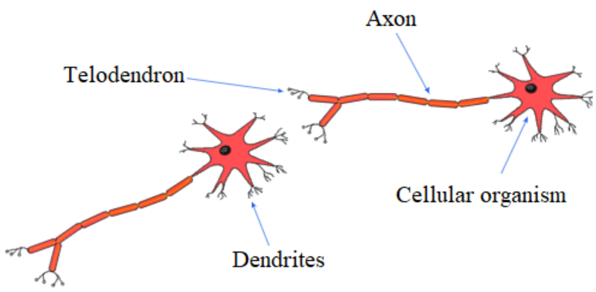

Figure 16: Representation of a biological neuron. Source: [Valenca, 2008].

The first to propose this biological neuron in an artificial model were McCulloch and Pitts [1943], and the model of this neuron is presented in Figure 17. Valenca [2008] states that this model looks for the biological neuron from a representation model.

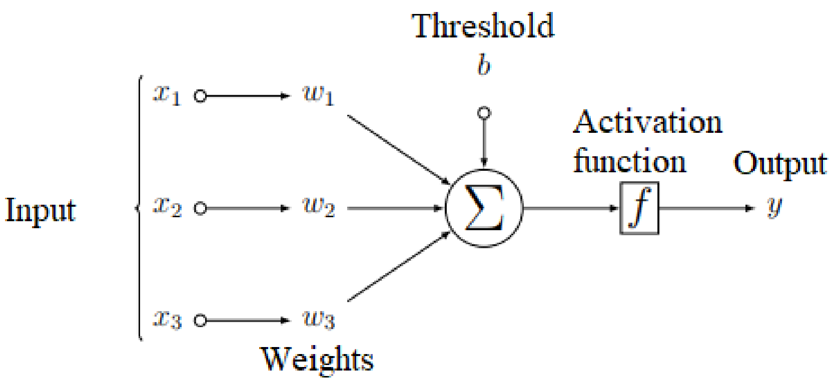

Figure 17: Threshold Logic Unit by McCulloch and Pitts. Source: [Bezerra, 2016].

Thus, consider x_1, x_2, x_3, to be the input variables of the output neuron y. The following propagation rule gives the $\sum$ entry:

$$\sum_{i=1}^{3} w_i x_i - b,$$

where w_i are the synaptic weights and b is the excitatory threshold. From this, it is possible to calculate the $f(\sum)$, known as the activation function, thus giving the desired output $y = f(\sum)$.

Neural networks are commonly structured in layers, where each unit can be related to units in the previous layer. There are the input layers, in which the patterns are indicated to the network, the intermediate or hidden layers, where most of the network's learning processing is performed, and the output layer, which presents the final result [Antognetti and Milutinovic, 1991].

There are two steps in developing an ANN: learning and use carried out sequentially and separately. In the learning stage, the data entered are visualized in two sets. The first group adjusts the network weights, while the second evaluates the training quality. Then, the utilization step is the mode in which the network corresponds to the input stimulus, not making further adjustments to its parameters [Braga et al., 2000].

In the case of ANFIS, in its training, it is necessary to use the method of least squares and gradient descent .

ANFIS, developed by Jang [1993], is a neuro-fuzzy system used to adjust membership functions and rules of an SBRF to find the most suitable answer for this system [Sodre et al., 2016]. The theory will be presented in the following subsection (subsection 3.2).

3.2 ANFIS

ANFIS is an artificial neural network of five layers interconnected through unit weights. Each layer is responsible for an operation that will produce an output equivalent to the one found at a given stage of a Takagi-Sugeno-type fuzzy system. Figure 18 is shown the equivalent architecture of ANFIS. To facilitate the understanding of the neuro-fuzzy network, we present a schema containing only two inputs, x_1 and x_2, and an output, y.

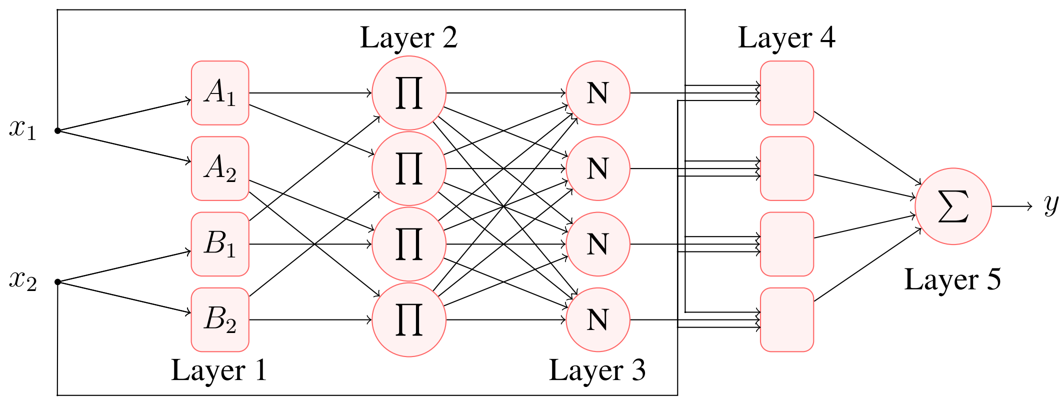

Figure 18: ANFIS architecture.

ANFIS implements four Takagi-Sugeno-type fuzzy rules:

Rule 1:	If (x_1 is A_1) and (x_2 is B_1)	then	$y = f_1 = k_{10} + k_{11}x_1 + k_{12}x_2;$
Rule 2:	If (x_1 is A_2) and (x_2 is B_2)	then	$y = f_2 = k_{20} + k_{21}x_1 + k_{22}x_2;$
Rule 3:	If (x_1 is A_2) and (x_2 is B_1)	then	$y = f_3 = k_{30} + k_{31}x_1 + k_{32}x_2;$
Rule 4:	If (x_1 is A_1) and (x_2 is B_2)	then	$y = f_4 = k_{40} + k_{41}x_1 + k_{42}x_2;$

where A_1 and A_2 are fuzzy sets of the universe X_1; B_1 and B_2 are fuzzy sets of the universe X_2; and k_{i0}, k_{i1} and k_{i2} are the parameter sets of rule i. Figure 7 shows the mechanism to obtain the inference method from the rules (9).

According to [Jang, 1993], after reading the data, its values are computed by membership functions that will identify the compatibility of each entry with its respective linguistic terms associated with this node. The function that is calculated in this layer is given by:

$$\begin{aligned} y_i^{(1)} &= \mu_{A_i}(x_1) \text{ for } i = 1, 2 \text{ ou} \\ y_i^{(1)} &= \mu_{B_{i-2}}(x_2) \text{ for } i = 3, 4, \end{aligned}$$

where x_1 or x_2 is an input of node i, A_i or B_{i-2} is the fuzzy set related to this node and $y_i^{(1)}$ is the output on the first layer.

For better understanding, we will assume that the membership functions are of the Gaussian type, according to the following equation:

$$\mu(x) = e^{-\frac{1}{2}\left(\frac{x-a}{b}\right)^2} \tag{9}$$

Note that each neuron in this layer has membership functions as its activation function in which the parameters of each of these functions are adaptive. It means that the parameters a and b are adjustable.

In the second layer, neurons have non-tunable activation functions $\prod$. In an ANFIS, the conjunction of rule antecedents is evaluated by the product of the operator (using some $t-$norm), where the output is given by:

$$\begin{aligned} y_1^{(2)} &= w_1 = \mu_{A_1}(x_1) \cdot \mu_{B_1}(x_2), \\ y_2^{(2)} &= w_2 = \mu_{A_1}(x_1) \cdot \mu_{B_2}(x_2), \\ y_3^{(2)} &= w_3 = \mu_{A_2}(x_1) \cdot \mu_{B_1}(x_2), \\ y_4^{(2)} &= w_4 = \mu_{A_2}(x_1) \cdot \mu_{B_2}(x_2), \end{aligned}$$

where $y_i^{(2)}$ is the output of this neuron obtained by the $t-$norm of the algebraic product.

In the third layer, there is another layer with fixed nodes, called N, non-adjustable, which normalizes the degrees of pertinence of each rule. Its function is given by:

$$y_i^{(3)} = \overline{w}_i = \frac{w_i}{w_1 + w_2 + w_3 + w_4}, i = 1, 2, 3, 4.$$

In the fourth layer, we have adaptive nodes again, whose function is composed of a set of parameters (k_{i0}, k_{i1} and k_{i2}) called consequent parameters. These parameters appear linearly in the output of each rule, according to the following function:

$$y_i^{(4)} = \overline{w}_i f_i = \overline{w}_i(k_{i0}x_1 + k_{i1}x_2 + k_{i2}),$$

where $\overline{w}_i$ is the activation level calculated in the previous layer.

Finally, in the last layer, there is, again, a layer with a single fixed node called $\sum$, in which the correct output of the neuro-fuzzy system is calculated, encompassing all inputs given by the function:

$$y_i^{(5)} = \sum_{i=1}^{4} \overline{w}_i f_i = \frac{\sum_{i=1}^{4} w_i f_i}{\sum_{i=1}^{4} w_i}.$$

ANFIS uses a hybrid learning algorithm that combines the least squares estimator and the [Jang, 1993] gradient descent method. First, initial activation functions are assigned to each associated neuron. The centers of the functions of the neurons connected to the input x_i are defined so that the domain of x_i is divided equally, and the widths and slopes are defined to allow sufficient overlap of the respective functions.

In the ANFIS training algorithm, each epoch comprises one step forward and one step back. In the forward pass, a training set of input patterns (an input vector) is presented to ANFIS. The neuron outputs are calculated layer by layer, and the consequent parameters of the rule are identified by the least-squares estimator. The antecedent parameters are adjusted through the error backpropagation algorithm. The following shows how this training takes place.

In the Takagi-Sugeno inference method, as shown in Figure 7, an output, f, is a linear function. Thus, given the values of the membership parameters and joint training of input-output patterns $p = 1, \cdots, P$, we can form linear equations P in terms of the consequent parameters as:

$$\begin{cases} Y_d(1) = \overline{w}_1(1)f_1(1) + \overline{w}_2(1)f_2(1) + \cdots + \overline{w}_n(1)f_n(1) \\ Y_d(2) = \overline{w}_1(2)f_1(2) + \overline{w}_2(2)f_2(2) + \cdots + \overline{w}_n(2)f_n(2) \\ \vdots \\ Y_d(p) = \overline{w}_1(p)f_1(p) + \overline{w}_2(p)f_2(p) + \cdots + \overline{w}_n(p)f_n(p) \\ \vdots \\ Y_d(P) = \overline{w}_1(P)f_1(P) + \overline{w}_2(P)f_2(P) + \cdots + \overline{w}_n(P)f_n(P) \end{cases} \tag{10}$$

or

$$\begin{cases} \begin{aligned} Y_d(1) &= \overline{w}_1(1)[k_{10} + k_{11}x_1(1) + k_{12}x_2(1) + \cdots + k_{1m}x_m(1)] \\ &+\overline{w}_2(1)[k_{20} + k_{21}x_1(1) + k_{22}x_2(1) + \cdots + k_{2m}x_m(1)] + \cdots \\ &+\overline{w}_n(1)[k_{n0} + k_{n1}x_1(1) + k_{n2}x_2(1) + \cdots + k_{nm}x_m(1)] \\ Y_d(2) &= \overline{w}_1(2)[k_{10} + k_{11}x_1(2) + k_{12}x_2(2) + \cdots + k_{1m}x_m(2)] \\ &+\overline{w}_2(2)[k_{20} + k_{21}x_1(2) + k_{22}x_2(2) + \cdots + k_{2m}x_m(2)] + \cdots \\ &+\overline{w}_n(2)[k_{n0} + k_{n1}x_1(2) + k_{n2}x_2(2) + \cdots + k_{nm}x_m(2)] \\ &\vdots \\ Y_d(p) &= \overline{w}_1(p)[k_{10} + k_{11}x_1(p) + k_{12}x_2(p) + \cdots + k_{1m}x_m(p)] \\ &+\overline{w}_2(p)[k_{20} + k_{21}x_1(p) + k_{22}x_2(p) + \cdots + k_{2m}x_m(p)] + \cdots \\ &+\overline{w}_n(p)[k_{n0} + k_{n1}x_1(p) + k_{n2}x_2(p) + \cdots + k_{nm}x_m(p)] \\ &\vdots \\ Y_d(P) &= \overline{w}_1(P)[k_{10} + k_{11}x_1(P) + k_{12}x_2(P) + \cdots + k_{1m}x_m(P)] \\ &+\overline{w}_2(P)[k_{20} + k_{21}x_1(P) + k_{22}x_2(P) + \cdots + k_{2m}x_m(P)] + \cdots \\ &+\overline{w}_n(P)[k_{n0} + k_{n1}x_1(P) + k_{n2}x_2(P) + \cdots + k_{nm}x_m(P)] \end{aligned} \end{cases} \tag{11}$$

where m is the number of input variables, n is the number of neurons in the third layer, and $Y_d(p)$ is the desired overall ANFIS output for inputs $x_1(p), \cdots, x_n(p)$.

The equation (11) can be written as follows:

$$y_d = Ak, \tag{12}$$

where y_d is a desired $P \times 1$ output vector,

$$y_d = \begin{bmatrix} Y_d(1) \\ Y_d(2) \\ \vdots \\ Y_d(p) \\ \vdots \\ Y_d(P) \end{bmatrix}_{P\times 1},$$

A is an matrix $P \times n(1+m)$,

$$A = \begin{bmatrix} \overline{w}_1(1) & \overline{w}_1(1)x_1 & \cdots & \overline{w}_1(1)x_m(1) & \cdots & \overline{w}_n(1)x_1(1) & \cdots & \overline{w}_n(1)x_m(1) \\ \overline{w}_1(2) & \overline{w}_1(2)x_1 & \cdots & \overline{w}_1(2)x_m(2) & \cdots & \overline{w}_n(2)x_1(2) & \cdots & \overline{w}_n(2)x_m(2) \\ \vdots & \vdots & \cdots & \vdots & \cdots & \vdots & \vdots & \vdots \\ \overline{w}_1(p) & \overline{w}_1(p)x_1 & \cdots & \overline{w}_1(p)x_m(p) & \cdots & \overline{w}_n(p)x_1(p) & \cdots & \overline{w}_n(p)x_m(p) \\ \vdots & \vdots & \cdots & \vdots & \cdots & \vdots & \vdots & \vdots \\ \overline{w}_1(P) & \overline{w}_1(P)x_1 & \cdots & \overline{w}_1(P)x_m(P) & \cdots & \overline{w}_n(P)x_1(P) & \cdots & \overline{w}_n(P)x_m(P) \end{bmatrix}_{P\times n(1+m)}$$

and k is a vector $n(1+m) \times 1$ of unknown consequent parameters

$$k = \begin{bmatrix} k_{10} & k_{11} & k_{12} & \cdots & k_{1m} & k_{20} & k_{21} & k_{22} & \cdots & k_{2m} & \cdots & k_{n0} & k_{n1} & k_{n2} & \cdots & k_{nm} \end{bmatrix}^T.$$

Typically, the number of input-output patterns P used in training is greater than the number of consequent parameters $n(1+m)$. This means that we are dealing with an overdetermined problem, so the exact solution to the equation (12) may not even exist. Thus, one must find a least-squares solution k^* that minimizes the quadratic error $||Ak - y_d||$, determined by:

$$k^* = (A^T A)^{-1} A^T y_d, \tag{13}$$

where, A^T is the transpose of A, and $(A^T A)^{-1} A^T$ is the pseudo-inverse of A if $(A^T A)$ is not singular. Once the consequent parameters of the rule are established, we can calculate a real network output vector, y, and determine the error vector e,

$$e = y_d - y,$$

so the backward propagation algorithm step is applied. Error signals are propagated back, and antecedent parameters are updated according to the chain rule.

It is considered a correction applied to the parameters a and b of the Gaussian activation function, equation (9), used in the neuron A_i. The chain rule is expressed according to the equations (15) and (16), for the parameters a and b, respectively. The squared error value E for the output neuron of ANFIS is given by:

$$E = \frac{1}{2}e^2 = \frac{1}{2}(y_d - y)^2. \tag{14}$$

According to Sandmann [2006], the partial derivatives are given by:

$$\frac{\partial E}{\partial a} = \frac{\partial E}{\partial e} \cdot \frac{\partial e}{\partial y} \cdot \frac{\partial y}{\partial(\overline{w}_i f_i)} \cdot \frac{\partial(\overline{w}_i f_i)}{\partial \overline{w}_i} \cdot \frac{\partial \overline{w}_i}{\partial w_i} \cdot \frac{\partial w_i}{\partial \mu_{A_i}} \cdot \frac{\partial \mu_{A_i}}{\partial a}. \tag{15}$$

$$\frac{\partial E}{\partial b} = \frac{\partial E}{\partial e} \cdot \frac{\partial e}{\partial y} \cdot \frac{\partial y}{\partial(\overline{w}_i f_i)} \cdot \frac{\partial(\overline{w}_i f_i)}{\partial \overline{w}_i} \cdot \frac{\partial \overline{w}_i}{\partial w_i} \cdot \frac{\partial w_i}{\partial \mu_{A_i}} \cdot \frac{\partial \mu_{A_i}}{\partial b}. \tag{16}$$

note that

$$\frac{\partial E}{\partial e} = \partial\left(\frac{1}{2}(e^2)\right) = e; \tag{17}$$

$$\frac{\partial e}{\partial y} = \frac{\partial(y_d - y)}{\partial y} = -1; \tag{18}$$

$$\frac{\partial y}{\partial(\overline{w}_i f_i)} = \frac{\partial\left(\sum_{i=1}^{n} \overline{w}_i f_i\right)}{\partial(\overline{w}_i f_i)} = 1; \tag{19}$$

$$\frac{\partial(\overline{w}_i f_i)}{\partial \overline{w}_i} = f_i; \tag{20}$$

$$\frac{\partial \overline{w}_i}{\partial w_i} = \frac{\partial\left(\frac{w_i}{\sum_{j=1}^{n} w_i}\right)}{\partial w_i} = \frac{\left(\sum_{j=1}^{n} w_j\right) - w_i}{\left(\sum_{j=1}^{n} w_j\right)^2} = \frac{\overline{w}_i(1-\overline{w}_i)}{w_i}; \tag{21}$$

$$\frac{\partial w_i}{\partial \mu_{A_i}} = \frac{w_i}{\mu_{A_i}}; \tag{22}$$

$$\frac{\partial \mu_{A_i}}{\partial a} = \left(e^{-\frac{1}{2}\left(\frac{x-a}{b}\right)^2}\right)a = e^{-\frac{1}{2}\left(\frac{x-a}{b}\right)^2}\left(\frac{(x-a)}{b^2}\right); \tag{23}$$

$$\frac{\partial \mu_{A_i}}{\partial b} = \frac{\partial(e^{-\frac{1}{2}\left(\frac{x-a}{b}\right)^2})}{\partial b} = e^{-\frac{1}{2}\left(\frac{x-a}{b}\right)^2}\left(\frac{(x-a)^2}{b^3}\right). \tag{24}$$

$$\tag{25}$$

The expressions of a and b, considering the learning rate α, will be corrected using the equations (15) and (16), given by:

$$a = a + \alpha(y_d - y) f_i \overline{w}_i (1-\overline{w}_i) \cdot \frac{1}{\mu_{A_i}} \cdot e^{-\frac{1}{2}\left(\frac{x-a}{b}\right)^2}\left(\frac{(x-a)}{b^2}\right), \tag{26}$$

$$b = b + \alpha(y_d - y) f_i \overline{w}_i (1-\overline{w}_i) \cdot \frac{1}{\mu_{A_i}} \cdot e^{-\frac{1}{2}\left(\frac{x-a}{b}\right)^2}\left(\frac{(x-a)^2}{b^3}\right). \tag{27}$$

Thus, according to ANFIS suggested by Jang [1993], it is verified that both the antecedent parameters and the consequent parameters are optimized. In the forward pass, the consequent parameters are adjusted while the antecedent parameters remain fixed. In the backward pass, the antecedent parameters are adjusted while the consequent parameters are kept fixed. According to Negnevitsky [2005], in some cases, when the input and output datasets are relatively small, membership functions can be described by a human expert. In such situations, these membership functions are kept fixed throughout the training process, and only the consequent parameters are adjusted.

In the sections 4 and 5 are shown ANFIS applications using experiments related to SHM.

4 ANFIS: Application in Temperature Compensation

This section presents an example that aims to perform data normalization, that is, to correct conditions that affect the signatures collected through the electromechanical impedance-based SHM technique, especially temperature.

4.1 The Experiment

The data used in this study come from an experiment carried out to investigate the ability of the electromechanical impedance technique to detect corrosion-associated failures in steel beams. The corrosion process is gradual and permanent and promotes increasing wear. In a long-term experiment, the beams were subjected to corrosion in an environment outside the laboratory through exposure to acid mist, while the impedance was measured cyclically. Acid mist induces corrosion acceleration. Results obtained from the analysis of this experiment were published by Freitas et al. [2021a].

A PZT patch was bonded to each beam to collect impedance signatures. Each impedance signature was measured with 8,000 frequency samples. The impedance analyzer used was developed by Finzi Neto et al. [2010], which is a portable and low-cost device.

Three specimens (steel beams 1020) with dimensions of $300mm \times 50mm \times 3.06mm$ and a mass of $354.15g$ were instrumented with PZT patches, with a diameter of $30mm$ and a thickness of $2mm$ each. The PZT patches were bonded with epoxy resin-based adhesive and subsequently protected with a sealant. A temperature sensor was coupled to each of the three specimens to compensate the measurements for the effect of temperature variation on the signals obtained. Figure 19a illustrates specimens instrumented with PZT patches.

Then, the samples were lightly sanded to remove the oxide layers formed and to set the initial pristine condition (baseline).

An acid mist was used, which reacted with the specimens, as a corrosive agent. To this end, a structure located outside the laboratory building was adapted to contain the specimens in an airtight environment, in a place with restricted access. In addition, this environment had a cover to protect against gusts of strong winds and rain. For better control of the corrosive mist action environment, a control box was developed, designed in a 3D design software as shown in Figure 19b.

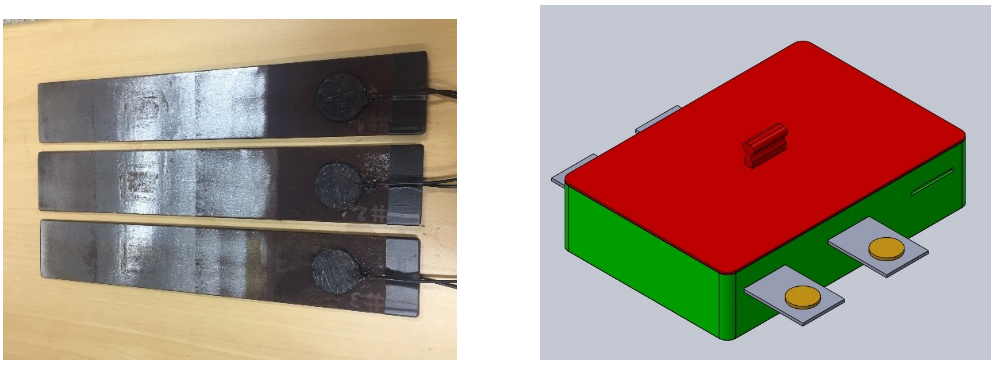

a: Specimens instrumented with PZT patches.

b: Control box used in the acid mist experiment.

Figure 19: Instrumented specimens and control box. Source: Freitas et al. [2021a].

Figure 19b represents the box that delimits an intermediate and considerable region of the specimens that remain subject to corrosive mist. Inside the box, small reservoirs were developed to add a small amount of hydrochloric acid, providing a corrosive environment. The control box was built in 3D printing. The final assembly of the experiment can be seen in Figures 20a and 20b.

a: Beams inside the control box.

b: Cable details and temperature sensor.

Figure 20: Control box. Source: Adapted from Freitas et al. [2021a].

The location of the temperature sensor, with the wire in white, can be seen by the red circle in Figure 20b

As stated earlier, temperature changes play an essential role in the damage detection process of the electromechanical impedance-based SHM method. The impedance signature of a structure can be different, even under the same structural conditions but at different temperatures. These differences are seen as horizontal and vertical displacements along with the signatures. Most of this variation is attributed to the temperature variation, as this variable interferes with the impedance value. If there is an important relationship between impedance and temperature, then it is possible to make predictions for impedance at temperatures not recorded in the experiment.

4.2 FRBSs Modeling

The FRBSs were modeled considering temperature and frequency as input variables. It was observed, through empirical tests, that the best setup consists of only two frequency values (points) per FRBSs, totaling 4,000 SBRFs. The output variable was impedance with a value at each frequency and temperature combination.

The data acquisition hardware stores the temperature values for each impedance reading per PZT patch. Therefore, each PZT patch has a set of temperature values corresponding to each impedance signal measured. In the validation process, part of the data set obtained in the baseline measurements was used to train and get the FRBSs. The other part for calculating damage indices, in which the signatures collected and modeled from the data set were used. FRBSs, at the respective temperatures. The temperatures in each of the two groups are shown in Table 3. Figure 21 shows the schematic of the mathematical modeling of the two phases that make up the experiment, in which the red rectangle represents the data obtained in the investigation; the blue rectangles represent the stage of training and construction of the FRBSs; and, in green, the validation step.

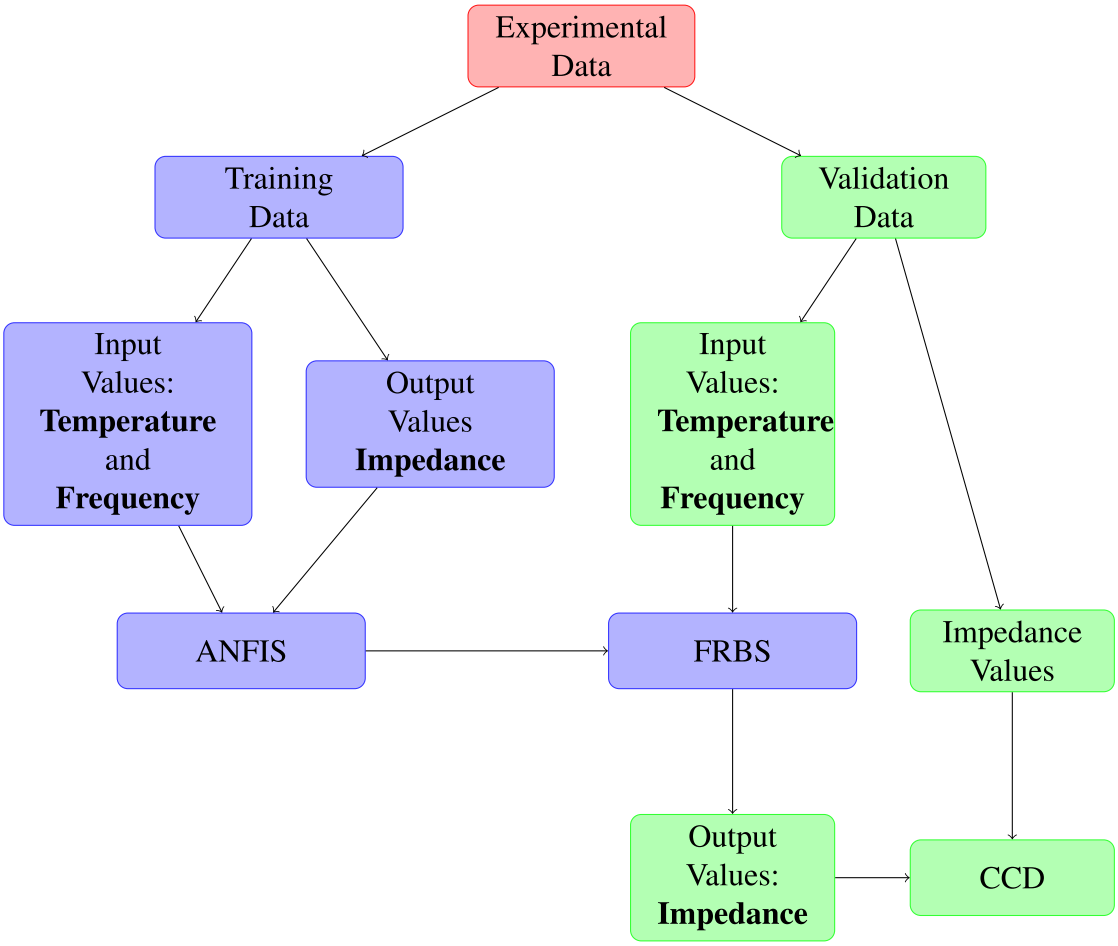

Figure 21: Scheme of the mathematical modeling used for the experiment.

To assess the quality of the models, the CCD metric was calculated from the pairs of baseline signatures measured and modeled from the SBRFs, at the same temperature. Low values of the CCD metric indicate the adequacy of the models or that the constructed signatures configure baseline signatures.

In the damage detection step, all temperatures observed in the baseline collection were used to train the FRBSs. For the second input variable, frequency, as in the validation step, two consecutive values were used in each FRBS. At this step, the output variable's impedance values were also observed in all frequency and temperature combinations.

The automation of building FRBSs for all frequency point pairs is relevant since the number of points used is generally significant. An iterative process was implemented in the software R [R Core Team, 2020] to obtain the 4000 FRBSs built from ANFIS through the package ANFIS [Fresno et al., 2015]. The R software allows the export of the FRBS built in each iteration to, for example, predict the impedance signatures at temperatures that can be observed in future investigations of the state of the structure.

4.3 Results: Model Evaluation

From the experimental data composed of 450 baseline signatures, each one with 8,000 frequency points, collected at temperatures between 23.7 to $31.3\,^{\circ}C$, 46 different temperatures were observed. The analysis was implemented from the median signature at each temperature. A median signature is defined by the set of median impedance values at each frequency point. For the three

PZT patches, the ANFIS training routine was programmed 4000 times, that is, to generate 4000 FRBSs. The training for the determination of the FRBSs was carried out considering two input variables and one output, as follows:

- First Input: For the temperature variable (t), the first and last values were considered, in ascending order, which corresponds respectively to $23.7\,°C$ and $31.3\,°C$, in addition to the temperatures corresponding to the exact positions of the 46 values, also arranged in ascending order. In this way, the extreme values were considered in training, ensuring that there was no validation data outside the training range;
- Second Input: For the frequency variable (f), two consecutive values were always used among the 8,000 values;
- Output: For the impedance variable (i), the values collected in the combination of the two input variables were considered, totaling 48 training values.

Temperatures not used in training were assigned for further validation. Table 3 shows the temperature values used in the training and validation of the PZT patches of the experiment.

Table 3: Temperatures (°C) recorded in the accelerated corrosion experiment.

PZT Patch	Set	Temperatures
1	Training	23.7 23.9 24.2 24.7 25.0 25.4 25.7 26.0 26.3 26.7 27.0 27.3 27.7 28.0 28.3 28.6 29.0 29.3 29.6 30.0 30.3 30.6 30.9 31.3
	Validation	24.0 24.4 24.9 25.2 25.5 25.8 26.2 26.5 26.8 27.2 27.5 27.8 28.1 28.5 28.8 29.1 29.5 29.8 30.1 30.5 30.8 31.1
2	Training	23.7 23.9 24.2 24.7 25.0 25.4 25.7 26.0 26.3 26.7 27.0 27.3 27.7 28.0 28.3 28.6 29.0 29.3 29.6 30.0 30.3 30.6 30.9 31.3
	Validation	24.0 24.4 24.9 25.2 25.5 25.8 26.2 26.5 26.8 27.2 27.5 27.8 28.1 28.5 28.8 29.1 29.5 29.8 30.1 30.5 30.8 31.1
3	Training	23.7 23.9 24.2 24.7 25.0 25.4 25.7 26.0 26.3 26.7 27.0 27.3 27.7 28.0 28.3 28.6 29.0 29.3 29.6 30.0 30.3 30.6 30.9 31.3
	Validation	24.0 24.4 24.9 25.2 25.5 25.8 26.2 26.5 26.8 27.2 27.5 27.8 28.1 28.5 28.8 29.1 29.5 29.8 30.1 30.5 30.8 31.1

Source: Adapted from Freitas et al. [2021a].

Thus, 4000 FRBSs were generated, all of which have two Gaussian membership functions for each input. The membership functions for temperature are the same for all FRBSs, as shown in Figure 22a. For frequency, the membership function centers on the fixed points of the experiment, as represented, for example, in Figure 22b. The four generated fuzzy rules, for PZT1 patch and frequencies 99990 and 100000, are described below:

Rule 1: If (t is High) and (f is High) then $i_1 = 0,3116833t + 0,00025376f + 2,5 * 10^{-9}$
Rule 2: If (t is Low) and (f is High) then $i_2 = 0,3134568t + 0,00025488f + 2,5 * 10^{-9}$
Rule 3: If (t is High) and (f is Low) then $i_3 = -0,02506984t + 0,00035051f + 3,5 * 10^{-9}$
Rule 4: If (t is Low) and (f is Low) then $i_4 = -0,01136947t + 0,00034594f + 3,4 * 10^{-9}$.

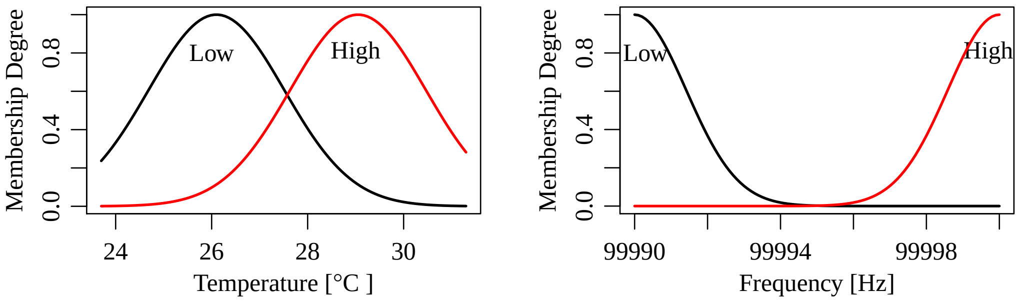

a: Membership functions for temperature. b: Membership functions for frequency.

Figure 22: Membership functions of FRBS inputs. Source: Adapted from Freitas et al. [2021a].

Figure 23 shows the surface generated from training step.

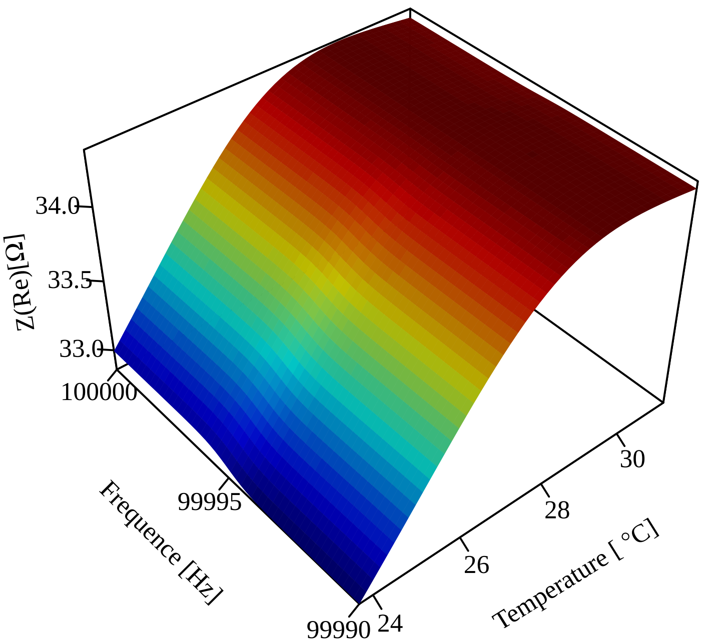

Figure 23: Surface built from an FRBS of the accelerated corrosion experiment, model evaluation step. Source: Freitas et al. [2021a].

The graphical validation was performed from the generated FRBSs, which consists of using an impedance signature of a given validation temperature from Table 3 with the signature predicted by the FRBSs at this same temperature. Three examples are shown in Figures 24, 25 and 26 for temperature values of $30.8\,°C$, $24.0\,°C$ and $27.2\,°C$ in PZT patches 1, 2 and 3, respectively. In addition to the graphical validation of the model, the validation is performed using the CCD values, according to the equation (3). Figure 27 presents the values obtained for the CCD damage metric for PZT patches 1, 2, and 3.

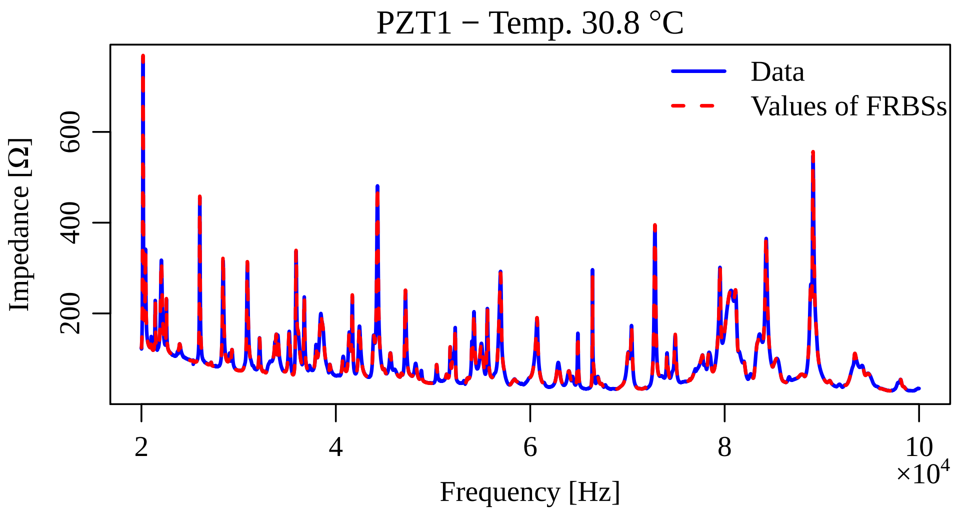

Figure 24: Impedance signatures measured and modeled from FRBSs, at temperature $30.8\,^{\circ}C$ in PZT1 patch

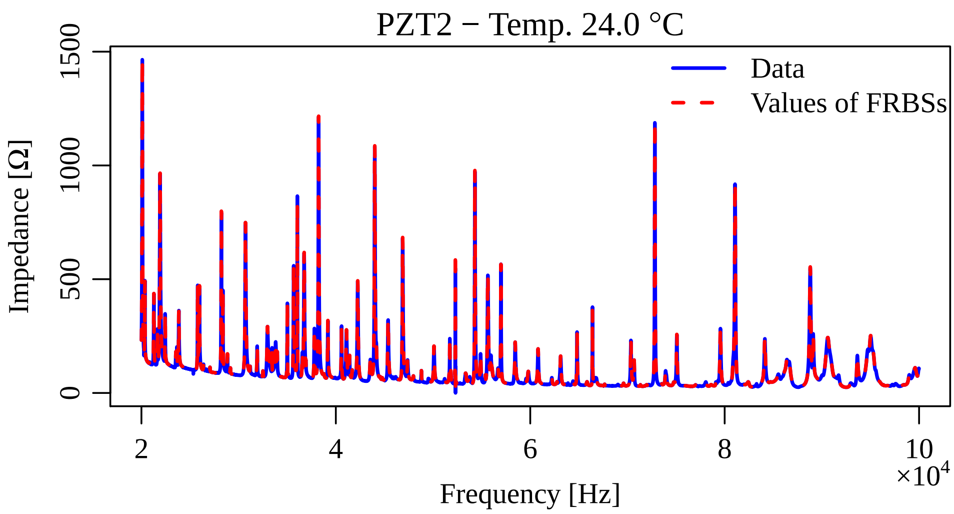

Figure 25: Impedance signatures measured and modeled from FRBSs, at temperature $24\,^{\circ}$C in PZT2 patch.

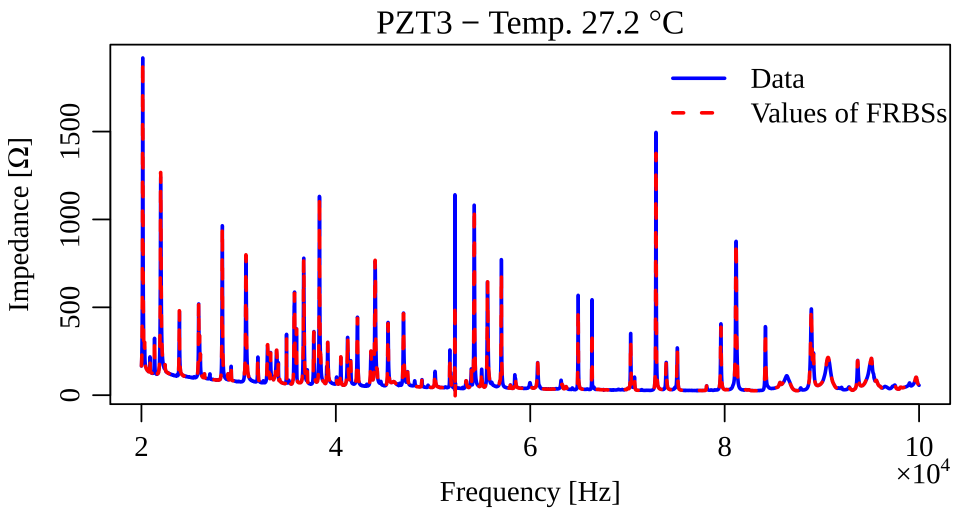

Figure 26: Impedance signatures measured and modeled from FRBSs, at temperature $27.2\,°\mathrm{C}$ in PZT3 patch.

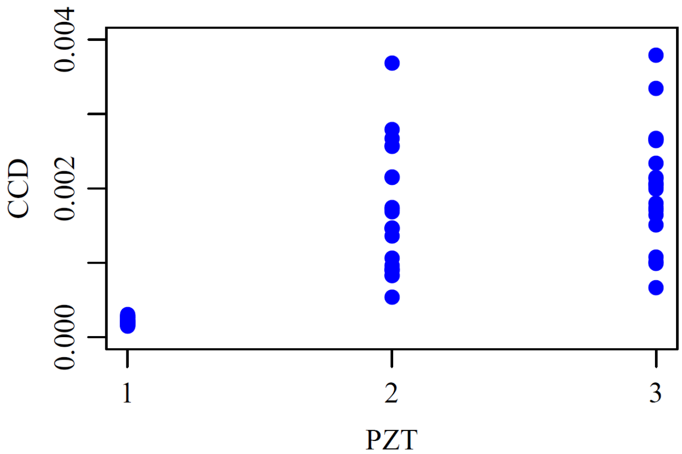

Figure 27: Baselines CCD metrics for the three PZT patches.

The highest CCD value was 0.003800021, and the difference between the impedance signatures collected and those predicted by the FRBSs is not significant (Figures 24, 25 and 26) and therefore built signatures configure baseline signatures.

4.4 Results: Damage Detection

Considering the same data from the first step and using the same settings for the SBRFs, two inputs (temperature and frequency) and one output (impedance), 4000 routines were performed for ANFIS training. All temperatures presented in Table 3 (training and validation), in this situation, were considered for training. Thus, 4000 FRBSs were generated, where the membership function for each entry has the same characteristics as those presented previously.

The four fuzzy rules generated for PZT1 patch and frequencies 99990 and 100000 are given by:

Rule 1:	If (t is High) and (f is High)	then	$i_1 = 0,4298513t + 0,0002239f + 2,2 * 10^{-9}$
Rule 2:	If (t is Low) and (f is High)	then	$i_2 = 0,4356641t + 0,0002240f + 2,2 * 10^{-9}$
Rule 3:	If (t is High) and (f is Low)	then	$i_3 = 0,0542666t + 0,0003258f + 3,2 * 10^{-9}$
Rule 4:	If (t is Low) and (f is Low)	then	$i_4 = 0,0706055t + 0,0003206f + 3,2 * 10^{-9}$.

Figure 28 shows the surface generated from training.

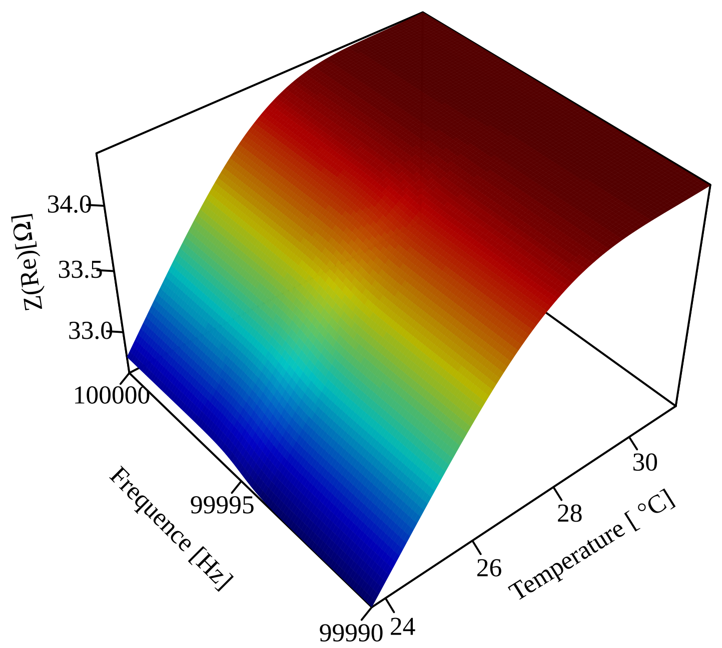

Figure 28: Surface generated from an SBRF from the accelerated corrosion experiment, damage detection step.

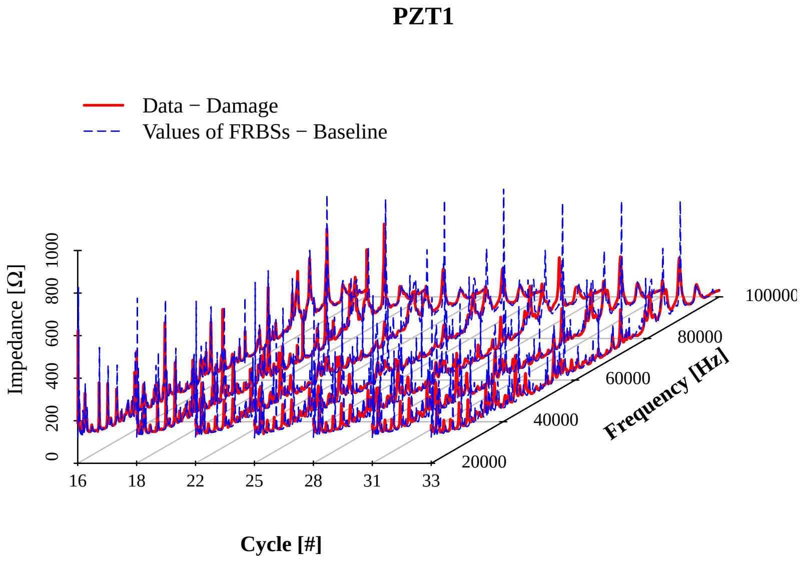

Figure 29: Impedance signatures, in some cycles, in the presence of damage and the corresponding baseline signature modeled from the FRBS, in PZT1 patch. Source: Adapted from Freitas et al. [2021a]

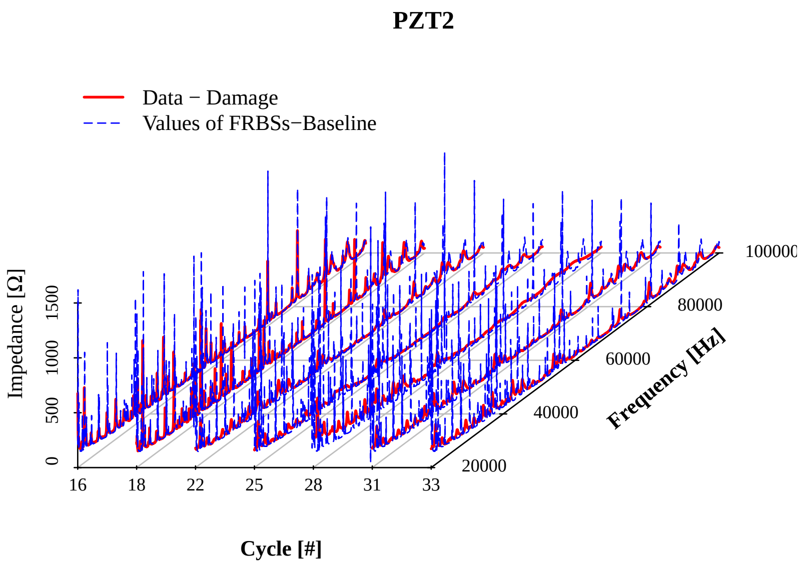

Figure 30: Impedance signatures, in some cycles, in the presence of damage and the corresponding baseline signature modeled from the FRBS, in PZT2 patch. Source: Adapted from Freitas et al. [2021a]

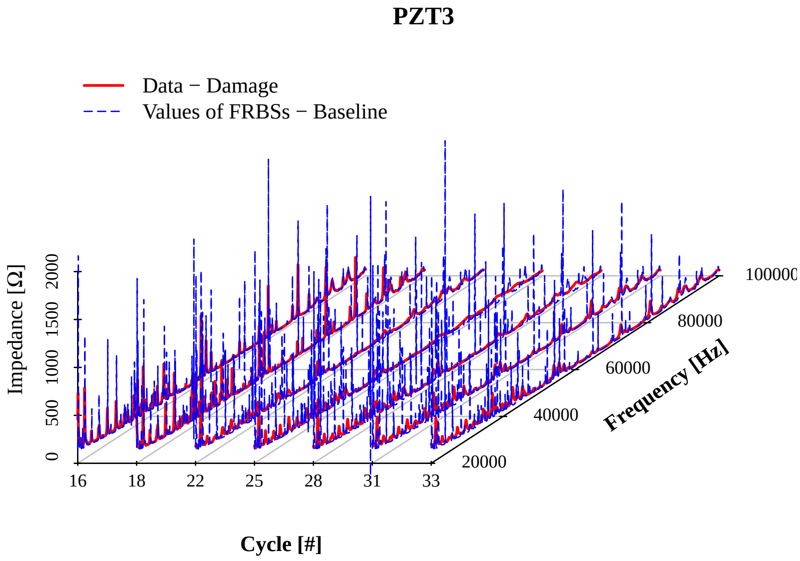

Figure 31: Impedance signatures, in some cycles, in the presence of damage and the corresponding baseline signature modeled from the SBRFs, in PZT3 patch. Source: Adapted from Freitas et al. [2021a]

For the validation part, a data set containing 33 distinct cycles were used, with 30 repetitions each, in which the first 14 cycles correspond to the original condition of the steel beams. In contrast, the acid mist was present in cycles 15 to 33, causing structural changes.

Figures 29, 30 and 31 show, in some corrosion cycles, a comparison of a signature with the damage corresponding to that cycle and a baseline signature modeled by the FRBSs, showing the difference between the measured signature and that provided by the FRBSs. This fact reveals that the methodology was able to distinguish baseline signatures from signatures with the presence of damage.

In Figures 32, 33 and 34 it is possible to observe the values of the CCD metric found according to the corrosion cycle. The cycles represent different moments of collection of impedance signatures due to the time elapsed in the execution of the experiment, called corrosion cycles. The CCD was calculated considering the median of the real signature collected in a given cycle and the signature of the baseline predicted by the SBRFs.

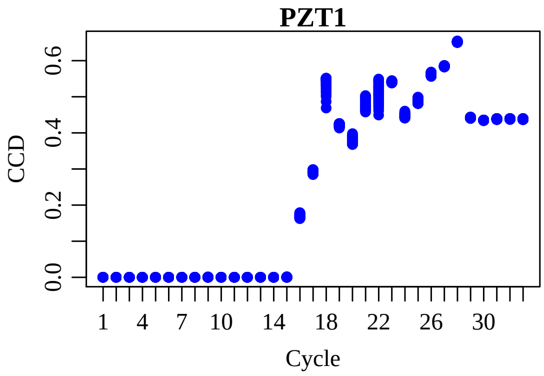

Figure 32: CCD values in the different conditions of the experiment in PZT1 patch. Source: Adapted from Freitas et al. [2021a]

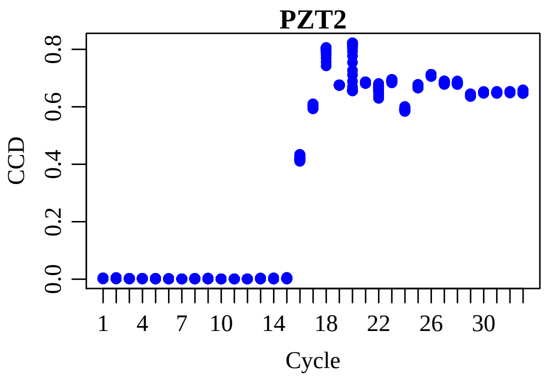

Figure 33: CCD values in the different conditions of the experiment in PZT2 patch. Source: Adapted from Freitas et al. [2021a]

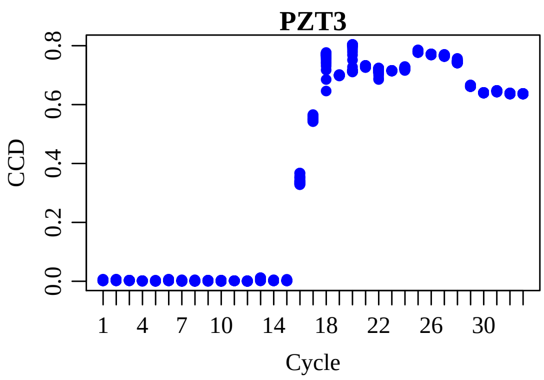

Figure 34: CCD values in the different conditions of the experiment in PZT3 patch. Source: Adapted from Freitas et al. [2021a]

The evolution of CCD values over the cycles indicates that the increase in acid caused a significant change in the values of this metric, mainly from the third cycle onwards. In cycles 15 and 16, this change was smaller, which is understandable, given that the acid action time, responsible for corrosion, was still small when compared to cycles identified by higher numbers. Another influence that must be considered is the accumulated oxides of the acid over time, which can affect the CCD value.

As mentioned, for the first phase, the model validation was perfect since the highest computed CCD was not significant and therefore did not indicate a structural change, which was expected given that the training and validation data were all baselines. The highest CCD baseline value obtained is 0.003800021, a shallow difference, meaning that the simulated signatures would be considered a sample of the actual baselines.

From the results presented in Figures 32, 33 and 34, it is possible to distinguish situations with damage, by the application of acid, from those without damage characterized by the absence of acid from the constructed FRBSs.

Therefore, the two steps of the experiment showed excellent results, providing an effective technique for data normalization.

5 ANFIS: Structural Change from the Increment of Mass

In this experiment is identified the level of damage in aluminum beams.

The experimental data used for the application of the methodology were obtained from eight specimens in an experiment in a climatic chamber (Figure 8), with temperature and humidity control installed in the Structural Mechanics Laboratory (LMEst) from the School of Mechanical Engineering of the Federal University of Uberlandia. This work was presented at the X Scientific Initiation Exhibition of FAMAT Freitas et al. [2021b].

5.1 Beams with added mass

A PZT patch was bonded to each beam to measure impedance signatures. Thus, the setup of the experiment began.

The specimens were aluminum beams 500 mm long, 38 mm wide, and 3.2 mm thick, and in each of these structures a 1 mm thick and 20 mm diameter PZT patch was bonded to 100 mm. from the end. The processes of promoting structural changes adopted were the addition of masses glued 380 mm from the center of the PZT patch at the opposite end of the beam. These specimens can be seen in Figure 35.

The experiment was carried out to use the addition of mass to change the structure behavior. Figure 35 shows the eight beams or specimens tested in the bi-supported boundary condition. A polystyrene foam (styrofoam) was used to make the base of the beams to reduce possible vibration transfer from the chamber and external environment to the specimens during measurements.

The experiment was carried out at temperatures -10, 0, 10, and $20°C$. For cases of damage by adding masses, five levels of failure were considered, the first being without additional mass (baseline signature) and four progressive levels. For a slight controlled variation in the experiment, the masses were added to the specimens according to Table 4.

Figure 35: Instrumented and identified beams.

Table 4: Mass values by damage level and beam.

	Baseline	Damage 1 (g)	Damage 2 (g)	Damage 3 (g)	Damage 4 (g)
Beam 1	No damage	0.6	1.1	1.6	2.2
Beam 2	No damage	0.6	1.1	1.6	2.2
Beam 3	No damage	0.6	1.1	1.6	2.8
Beam 4	No damage	0.6	1.1	1.6	2.7
Beam 5	No damage	0.6	1.1	1.6	2.2
Beam 6	No damage	0.6	1.1	1.6	2.2
Beam 7	No damage	0.6	1.1	1.6	2.2
Beam 8	No damage	0.6	1.1	1.6	2.2

As represented in Table 4, damage level 4 was not the same mass value in all beams. In Figure 36, it is possible to identify the different configurations, in three beams, for damage level 4.

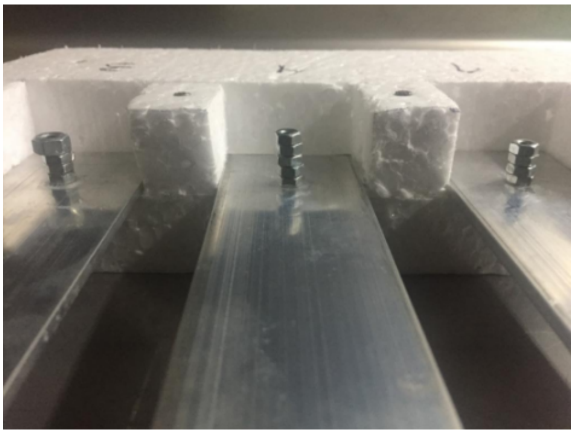

Figure 36: Different mass values: damage level 4, on beams 3, 4 and 1.

For each experimental condition, determined by the temperature value and damage level, 20 impedance signatures were collected in each of the eight beams, totaling 3200 signatures.

Previous exploratory analyses found that the data obtained in the PZT2 patch did not represent typical impedance signatures due to acquisition problems; therefore, these data were not used in the study.

5.2 FRBSs Evaluation and Modeling Criteria

One of the difficulties encountered in this methodology is quantifying the damage from the metrics since their behavior does not follow the change made in the structure.

The SBRFs modeled for this experiment consist of two inputs, CCD and $RMSD1$, calculated from the investigated signature and respective baseline.

In the validation step, the FRBS output value was compared using the pairs CCD and $RMSD1$, continuously computed with identical impedance signatures. Figure 37 presents a schematic of the mathematical modeling for the experiment, in which the red rectangle represents the data obtained in the investigation; the blue rectangles represent the stage of training and construction of the FRBSs, and in green the validation step.

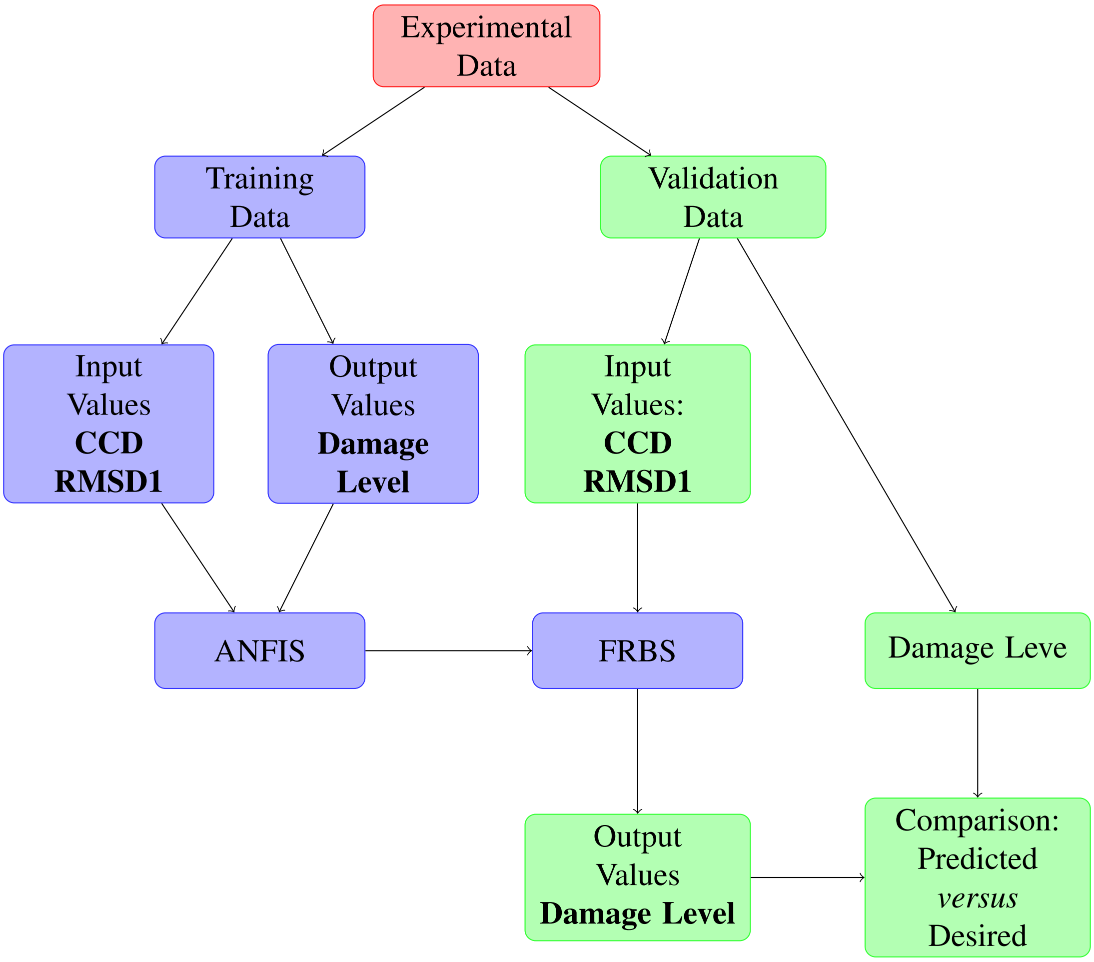

Figure 37: Scheme of the mathematical modeling used for the experiment

5.3 Results: Model evaluation

Considering the data set from the experiment for each PZT patch, the CCD (equation (3)) and RMSD1 (equation (1)) metrics are computed for each signature, which are the variables of SBRF entries. The output variable is the damage level obtained from Table 4, observed in the experiment by increasing the mass in the structure.

The training step in ANFIS (MATLAB) is performed by taking the even or odd indices of the combinations of CCD and RMSD1 metrics, taken according to the order of signature collections or, in some training, in ascending order of RMSD1 metric. The choice of the data set used in training is the one that best approached the expected results. Thus, data set not used in training were considered for validation. Therefore, the number of FRBSs built is 28, as four temperatures and seven PZT patches were considered in the study.

For the training of each model, different amounts of membership functions are configured. Figure 38 illustrates the membership functions generated by training in the PZT1 patch for a temperature of 20^oC. The input variables are:

- CCD values: the domain $[0, 0.52]$, representing the ranges $[0, 0.1]$, $[0.04, 0.22]$, $[0.17, 0.35]$, $[0.3, 0.48]$ and $[0.43, 0.52]$, with the linguistic terms: Very Low, Low, Medium, High and Very High, respectively.

- RMSD1 values: the domain $[1.25, 5402]$, representing the ranges $[1, 25, 757.3]$, $[325.3, 1837]$, $[1405, 2918]$, $[2486, 3998]$, $[3566.5078]$, $[4646.5402]$, with the linguistic terms: Very Low, Low, Medium, Medium High, High and Very High, respectively.

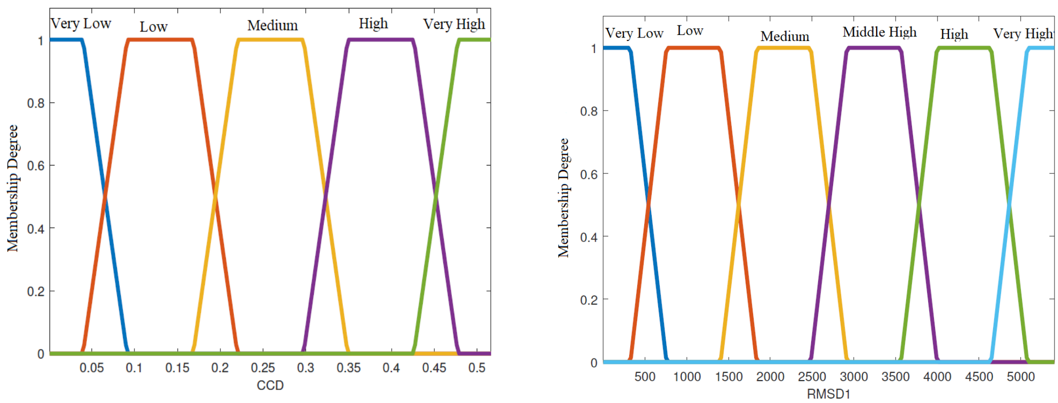

a: Membership functions to input CCD metric. b: Membership functions to input RMSD1 metric.

Figure 38: Membership functions to inputs.

Figure 39 shows the surface generated from training. The system generated 30 possible fuzzy rules and output function parameters.

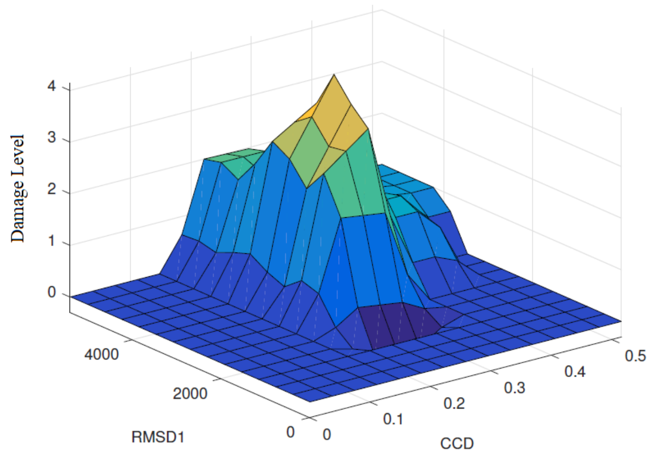

Figure 39: Surface generated from a FRBS. Source: Freitas et al. [2021a]

FRBSs are validated by approximating the output values of FRBSs by the nearest integer to the damage level 0, 1, 2, 3, or 4 and comparing it with the damage observed in the experiment. Furthermore, Table 5 presents the percentages of correct answers for the FRBSs, considering 50 values of CCD and RMSD1 metrics for each temperature and PZT patch.

Table 5: FRBSs hit percentages according to each temperature.

PZT Patch	Temperature [$^\circ C$]			
	-10	0	10	20
1	88%	96%	88%	100%
3	100%	90%	100%	98%
4	94%	100%	100%	100%
5	88%	94%	100%	100%
6	80%	96%	100%	100%
7	100%	92%	100%	94%
8	88%	88%	98%	88%

The results presented in Table 5 show that a high proportion of correct answers is obtained from the proposed model. The lowest hit percentage is 80% in the PZT6 patch with $-10^\circ C$, while in 12 PZT patches and temperature combinations, there was a 100% hit. The results obtained through the FRBSs showed that the technique could be a promising tool for damage detection since it achieved an average percentage of hits of 95%, comparing the predicted and the expected.

Finally, the next section addresses the conclusion of this chapter.

6 Concluding Remarks

ANFIS combines artificial intelligence and fuzzy set theory, providing efficient models for different problems. The combination of these two tools, through ANFIS, can improve the ability to represent and infer models.

In the application example, the methodology used for temperature compensation was efficient because the values of the CCD metric between the modeled signatures and the measured baseline signatures were low. Therefore, this approach through ANFIS is a suitable implementation of the baseline state representation. The proposed method is effective for data normalization, and it is possible to build reference signatures in the temperature range collected in the baseline gathering process. In other applications, wider temperature ranges can be considered, and these applications can be extended to different structures such as bridges, buildings, and tanks.

From the second application proposed in this chapter, it can be concluded that the percentage of correctness regarding the state of the structure was high, 95%. In this case, ANFIS was also used to model FRBSs in which the input variables were the CCD and the RMSD1 metrics.

The mathematical approach proposed in this chapter for the study of electromechanical impedance-based SHM provided promising results. This methodology allows the tuning of the functions of the input and output variables. It is a mathematical tool with great potential as it combines the learning characteristics of neural networks with the interpretability of Fuzzy Rule-Based Systems.

Acknowledgements

The authors are thankful to Petrobras for the financial support via the research project (RD).

References

K. E. I. Alfaro. Aplicações da extensão de zadeh na dinâmica do hiv com retardo fuzzy sob tratamento antirretroviral. Master's thesis, Universidade Federal de Uberlândia-UFU, 2019.

P. Antognetti and V. Milutinovic. Neural networks: Concepts, aplications, and implementations. *New Jersey: Prentice Hall*, page 310, 1991.

L. C. Barros and R. Bassanezi. *Tópicos de lógica fuzzy e biomatemática*. UNICAMP/IMECC, Campinas, SP, 2015.

A. Bastani, H. Amindavar, M. Shamshirsaz, and N. Sepehry. Identification of temperature variation and vibration disturbance in impedance-based structural health monitoring using piezoelectric sensor array method. *Structural Health Monitoring*, 11(3):305–314, 2012.

S. G. T. A. Bezerra. Reservoir computing com hierarquia para previsão de vazões médias diárias. Master's thesis, Universidade de Pernambuco, 2016.

S. Bhalla, A. S. K. Naidu, and C. K. Soh. Influence of structure-actuator interactions and temperature on piezoelectric mechatronic signatures for nde. In *Smart Materials, Structures, and Systems*, volume 5062, pages 263–269, Bangalore, India, 2003. International Society for Optics and Photonics.

A. P. Braga, A. C. P. L. F. Carvalho, and T. B. Ludemir. Redes neurais artificiais: Teoria e aplicações. *Rio de Janeiro: Livros Técnicos e científicos Editora S. A*, page 262, 2000.

D. P. L. Ferreira. Sistema p-fuzzy aplicado às equações diferenciais parciais. Master's thesis, Universidade Federal de Uberlândia - UFU, 2011.

R. M. Finzi Neto, V. Steffen, D. A. Rade, C. A. Gallo, and L. V. Palomino. A low-cost electromechanical impedance-based SHM architecture for multiplexed piezoceramic actuators. *Structural Health Monitoring*, 10:391–402, 2010. doi: 10.1177/1475921710379518.

C. A. G. Fonseca. Estrutura ANFIS modificada para identificação e controle de plantas com ampla faixa de operação e não linearidade acentuada. Master's thesis, Universidade Federal do Rio Grande do Norte - UFRGN, 2012.

F. A. Freitas. Aplicação da teoria dos conjuntos fuzzy no estudo da impedância eletromecânica. Master's thesis, FAMAT, Universidade Federal de Uberlândia, 2021.

F. A. Freitas, R. M. Jafelice, J. W. d. Silva, D. d. S. Rabelo, Q. S. S. Nomelini, J. d. R. V. d. Moura, C. A. Gallo, M. J. d. Cunha, and J. E. Ramos. A new data normalization approach applied to the electromechanical impedance method using adaptive neuro-fuzzy inference system. *Journal of the Brazilian Society of Mechanical Sciences and Engineering*, 43(11):1–13, 2021a.

F. A. Freitas, R. S. M. Jafelice, J. W. da Silva, C. A. Gallo, and J. E. Ramos. Detecção de danos em vigas de alumínio via modelagem fuzzy, 2021b. URL `http://www.eventos.ufu.br/sites/eventos.ufu.br/files/documentos/caderno_de_resumos_2021_0.pdf`. X Mostra de Iniciação Científica da FAMAT, Acesso: 28/06/2021.

F. A. Freitas et al. Aplicaçao da teoria dos conjuntos fuzzy no estudo da impedância eletromecânica. 2021c.

C. Fresno, A. S. Llera, and E. A. Fernandez. *ANFIS: Adaptive Neuro Fuzzy Inference System in R*, 2015. URL `https://CRAN.R-project.org/package=anfis`. R package version 0.99.1.

B. M. Gianesini, N. E. Cortez, R. A. Antunes, and J. Vieira Filho. Method for removing temperature effect in impedance-based structural health monitoring systems using polynomial regression. *Structural Health Monitoring*, 20(1):202–218, 2021.

R. S. M. Jafelice, L. C. de Barros, and R. C. Bassanezi. Teoria dos conjuntos fuzzy com aplicações (*e-book*). *São Carlos, SP: SBMAC*, 17:119, 2012.

J.-S. R. Jang. Adaptive-network-based fuzzy inference system. *IEEE Transactions on Systems, Man, and Cybernetics*, 3(23), 1993.

K.-Y. Koo, S. Park, J.-J. Lee, and C.-B. Yun. Automated impedance-based structural health monitoring incorporating effective frequency shift for compensating temperature effects. *Journal of intelligent material systems and structures*, 20(4):367–377, 2009.

K. Krishnamurthy, F. Lalande, and C. A. Rogers. Effects of temperature on the electrical impedance of piezoelectric sensors. In *Smart Structures and Materials 1996: Smart Structures and Integrated Systems*, volume 2717, pages 302–310. International Society for Optics and Photonics, 1996.

I. I. C. Maruo, G. de Faria Giachero, V. S. Júnior, and R. M. F. Neto. Electromechanical impedance - based structural health monitoring instrumentation system applied to aircraft structures and employing a multiplexed sensor array. *Journal of Aerospace Technology and Management*, pages 294–306, 2015. doi: 10.5028/jatm.v7i3.447.

W. S. McCulloch and W. Pitts. A logical calculus of the ideas immanent in nervous activity. *The bulletin of mathematical biophysics*, 5:115–133, 1943.

J. R. V. Moura and V. Steffen. Impedance-based health monitoring: Frequency band evaluation. *Proceedings of the 22nd International Modal Analysis Conference (IMAC XXII)*, 2004.

N. N. Nardez. Obtenção do parâmetro pco de antenas gnss por meio de sistemas baseado em regras fuzzy. Master's thesis, UFP, 2015.

M. Negnevitsky. *Artificial Inteligence: A Guide to Intelligent Systems*. Pearson Education Limited, Addison Wesley, 2 edition, 2005.

L. Palomino. Análise das métricas de dano associadas à técnica da impedância eletomecânica para o monitoramento de integridade estrutural. Master's thesis, Universidade Federal de Uberlândia - UFU, 2008.

G. Park, K. Kabeya, H. H. Cudney, and D. J. Inman. Impedance-based structural health monitoring for temperature varying applications. *JSME International Journal Series A Solid Mechanics and Material Engineering*, 42(2):249–258, 1999.

E. Pourjavad and A. Shahin. The application of Mamdani fuzzy inference system in evaluating green supply chain management performance. *International Journal of Fuzzy Systems*, 20(3): 901–912, 2018.

R Core Team. *R: A Language and Environment for Statistical Computing*. R Foundation for Statistical Computing, Vienna, Austria, 2020. URL `https://www.R-project.org/`.

D. S. Rabelo, K. M. Tsuruta, D. D. de Oliveira, A. A. Cavalini, R. M. F. Neto, and V. Steffen. Fault detection of a rotating shaft by using the electromechanical impedance method and a temperature compensation approach. *Journal of Nondestructive Evaluation*, 2017.

H. R. Sandmann. Predição não-linear de séries temporais usando sistemas de arquitetura neuro-fuzzy. Master's thesis, Escola Politécnica, Universidade de São Paulo, São Paulo, 2006.

N. Sepehry, M. Shamshirsaz, and F. Abdollahi. Temperature variation effect compensation in impedance-based structural health monitoring using neural networks. *Journal of Intelligent Material Systems and Structures*, 22(17):1975–1982, 2011.

R. N. F. Silva, K. M. Tsuruta, D. S. Rabelo, R. M. F. Neto, A. A. C. Jr., and V. S. Jr. Impedance-based structural health monitoring applied to steel fiber-reinforced concrete structures. *Journal of the Brazilian Society of Mechanical Sciences and Engineering*, page 42:383, 2020. doi: https://doi.org/10.1007/s40430-020-02458-4.

E. D. A. Sodre, W. S. Mota, and B. D. S. Alencar. Sistema híbrido neuro-*fuzzy* para análise de segurança em tempo real de sistemas de potência. *Congresso Brasileiro de Redes Neurais*, 8, 2016.

F. P. Sun, Z. Chaudhry, C. Liang, and C. Rogers. Truss structure integrity identification using pzt sensor-actuator. *Journal of Intelligent material systems and structures*, 6(1):134–139, 1995.

M. Valenca. *Fundamentos das Redes Neurais: exemplos em Java*. Recife, Editora Livro Rápido – Elógica, 2 edition, 2008.

L. Zadeh. Fuzzy sets. *Information and control*, 8(3):338–353, 1965.

D. Zhou, J. K. Kim, D. S. Ha, J. D. Quesenberry, and D. J. Inman. A system approach for temperature dependency of impedance-based structural health monitoring. In *Smart Sensor Phenomena, Technology, Networks, and Systems 2009*, San Diego, USA, 2009. International Society for Optics and Photonics.